PLOS ONE

RESEARCH ARTICLE

Geochemical characteristics and detrital zircon U-Pb ages of the Yimin Formation, Kelulun Depression, Hailar Basin and constraints on uranium mineralization

Fanmin Meng[1]*, Fengjun Nie[1,2]*, Fei Xia[1,2], Zhaobin Yan[1], Da Sun[1], Wenbo Zhou[3], Xin Zhang[1], Qing Wang[1]

1 School of Earth Sciences, East China University of Technology, Nanchang, Jiangxi Province, China, **2** State Key Laboratory of Nuclear Resources and Environment, East China University of Technology, Nanchang, Jiangxi Province, China, **3** Geological Party No. 243, CNNC, Chifeng, Inner Mongolia, China

* niefj@263.net (FN); 18702625683@163.com (FM)

Citation: Meng F, Nie F, Xia F, Yan Z, Sun D, Zhou W, et al. (2024) Geochemical characteristics and detrital zircon U-Pb ages of the Yimin Formation, Kelulun Depression, Hailar Basin and constraints on uranium mineralization. PLoS ONE 19(8): e0309433. https://doi.org/10.1371/journal.pone.0309433

Editor: Rizwan Sarwar Awan, Hefei University of Technology School of Resources and Environmental Engineering, CHINA

Received: June 4, 2024

Accepted: August 12, 2024

Published: August 30, 2024

Data Availability Statement: within the manuscript and/or Supporting Information files.

Funding: The major changes are marked in yellow in the manuscript. Secondly, the research is supported by Mechanism of constraints of the basin and range coupling on uranium mineralization in the southern Great Xing'an Range and its lateral basins (Project No. U2244205), Responses of accumulation of uranium and its

Abstract

The sandstone uranium deposits in the Kelulun Depression are the first commercially viable uranium deposits discovered in the Hailar Basin and the ore-bearing strata corresponding to the Lower Cretaceous Yimin Formation. However, the source of sedimentary matter, uranium source conditions, and uranium mineralization processes in the region have not been characterized. Accordingly, we analyzed the lithology, whole-rock geochemistry, zircon U-Pb ages, and trace elements of the Yimin Formation sandstones. The Yimin Formation sandstones were primarily composed of detrital grains with low compositional maturity. A geochemical analysis indicated that the parent rocks are felsic igneous rocks formed at an active continental margin with a moderately high degree of weathering. The detrital zircon U-Pb ages of the Yimin Formation 215–287 Ma with a peak at 230–260 Ma. Based on chronological, geochemical, and lithological data, we conclude that the Yimin Formation matter is derived from the Adunchulu Uplift on the western side of the Kelulun Depression and its parent rocks are Triassic granites. The Adunchulu uplift since the late Early Cretaceous and weathering and denudation of its uranium-rich granites provided ample matter and uranium. Therefore, the Kelulun Depression is a promising area for the exploration of sandstone uranium deposits.

1. Introduction

Sandstone uranium deposits are often very large, environmentally friendly to mine, and have low burial depths and mining costs. As such, they have become the primary focus of uranium exploration efforts across the world [1–3]. Large and ultra-large sandstone uranium deposits have been discovered in the Yili, Junggar, Ordos, Songliao, and Erlian Basins of China [4–11]. Recently, sandstone-related uranium deposits of considerable size have also been discovered in the Cretaceous strata of the Hailar Basin in northeastern Inner Mongolia.

associated elements in sandstone-type uranium deposit to tectonic inversion in the southern Songliao Basin (Project No. U2067202). The funders had no role in study design, data collection and analysis, decision to publish, or preparation of the manuscript.

Competing interests: The author has declared that there are no competing interests.

The Hailar Basin is rich in hydrocarbon resources, such as coal, petroleum, and natural gas [12]. Based on sandbody characteristics [13,14], hydrogeological conditions [15], airborne radiometric survey data [16], and prospecting analyses [17–19], the geological conditions of the Hailar Basin are conducive to uranium mineralization. Many uranium points and deposits have recently been discovered in the Lower Cretaceous Yimin Formation of the Kelulun Depression, in the southwestern part of the Hailar Basin. Meng (2024) used electron microprobe to reveal the types and occurrence states of uranium minerals in the Yimin Formation, and elemental geochemical characteristics revealed the rock types, tectonic setting, sedimentary environment and paleoclimatic conditions in the source area of the Yimin Formation [20]. However, the geochemical data can only be used to determine the parent rock type in the source area of the Yimin Formation, but cannot accurately pinpoint the provenance. The research level of the Yimin Formation strata in the area is still relatively low, especially the source of the clastic material, sedimentary system, uranium source conditions, and uranium mineralization mechanisms, limiting the exploration of sandstone-related uranium deposits in this area. To address this problem, we analyzed the lithology, geochemistry, and zircon U-Pb ages of samples from the Lower Cretaceous Yimin Formation in the Kelulun Depression to reveal the sources of detrital matter, lithology of the parent rock, and tectonic setting and uranium fertility of the source region. Uranium mineralization processes were then inferred from the tectonic evolution of the source region and the aforementioned analyses. The study results are expected to guide future explorations for sandstone uranium deposits in the Hailar Basin.

2. Geological background

The Hailar Basin, located in the eastern Central Asian Orogenic Belt (Fig 1A), is a Mesozoic-Cenozoic continental rift basin that developed between the Siberian and North China Plates [21–23]. The basin is controlled by the NE-striking Deerbugan and Ergun fault zones, and it has undergone four stages of tectonic evolution, a rifting stage in the Late Jurassic, a syn-rifting stage during the Early Cretaceous, a shrinking stage in the late Early Cretaceous, and differential uplift and denudation during the Late Cretaceous-Neogene [24–29], which formed a tectonic pattern with "two uplifts and three depressions." (Fig 1B) [30,31].

The Kelulun Depression is a long and narrow half-graben in the southwestern part of the Hailar Basin, which trends in the NE direction and is bounded by faults on its western side (Fig 1C). The basement of the basin is comprised of Paleozoic metamorphic rocks and Hercynian granites, with many granites and intermediate-to-acidic and intermediate-to-alkaline igneous rocks around the basin. In descending chronological order, its sedimentary strata are the Lower Cretaceous Nantun, Tongbomiao, Damoguaihe, and Yimin Formations, the Neogene Huchashan Formation, and Quaternary strata. The ore-bearing strata in the study area are the Lower Cretaceous Yimin Formation, consisting of dark coal-bearing clastic sediments with high reducing capacities. Uranium mineralization has been discovered in the fan deltas of the Yimin Formation.

3. Sample acquisition and analysis

Whole-rock geochemical analyses were performed on 24 sandstone samples from boreholes ZKH5-2, ZKH12-1, ZKKL332-23, and ZKKL99-51 in the Kelulun Depression, were obtained from gray-white sandstone in the Yimin Formation, via four boreholes. The sample locations are shown in Fig 1C. Preparation of the thin rock sections, the selection of zircons, target preparation, and cathodoluminescence (CL) microscopy were performed by the Langfang Geological Exploration Technology Service Co., Ltd.

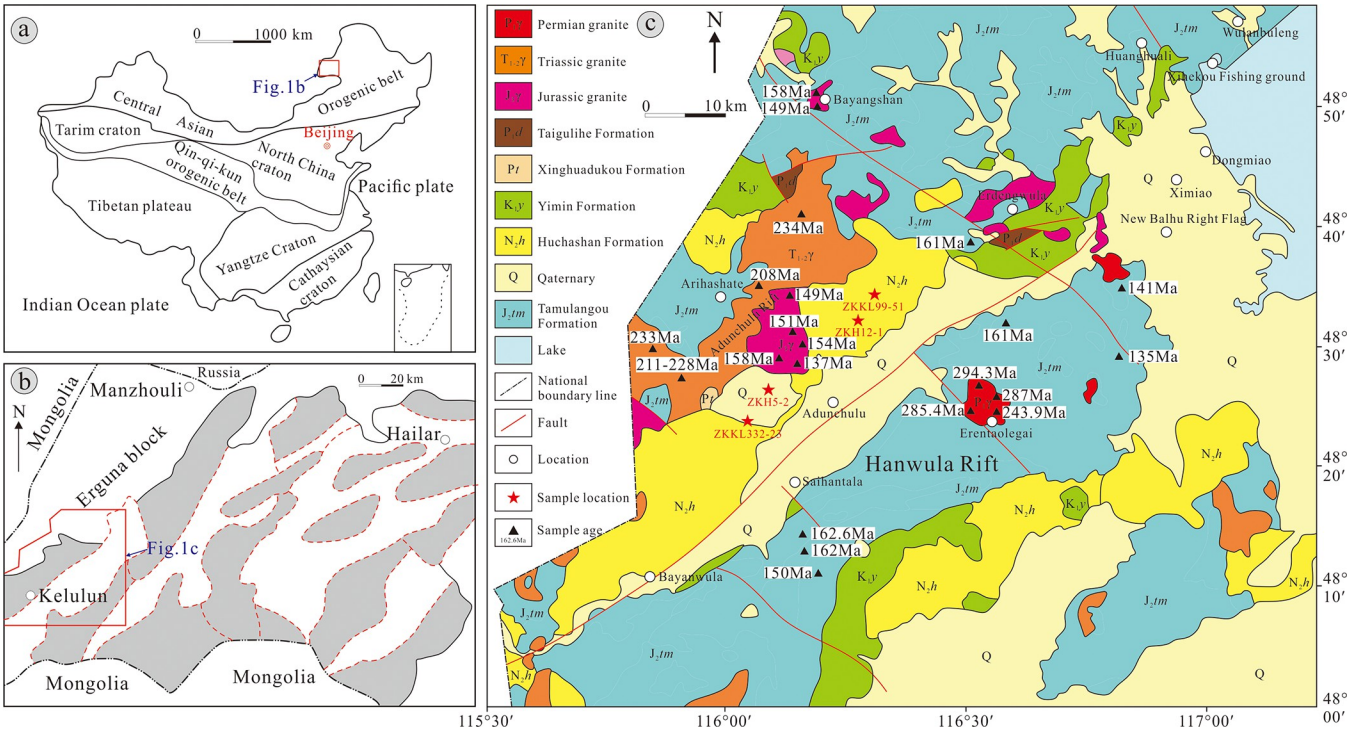

Fig 1. Geological map of the study area [20]. a. Geotectonic map of the Hailar Basin. b. Tectonic subdivisions of the Hailar Basin. c. Geological map of the Kelulun Depression. Republished from [Meng F.M, Nie F.J, Xia F, Yan Z.B, Sun, D, Zhou W.B, et al. Sedimentary Environment, Tectonic Setting, and Uranium Mineralization Implications of the Yimin Formation, Kelulun Depression, Hailar Basin, China. 2024; 12, 763.] under a CC BY license, with permission from [Journal of Marine Science and Engineering], original copyright [2024].

https://doi.org/10.1371/journal.pone.0309433.g001

3.1 Major and trace element analyses

Whole-rock geochemical analyses were performed at the Nuclear Geology and Nuclear Technology Application Center of Hunan Province. Major element analyses were performed using a Shimadzu XRF-1800 (Japan) X-ray fluorescence fluorometer, with an analytical accuracy of 5% or better. Trace and rare earth element analyses were performed via inductively coupled plasma mass spectrometry (ICP-MS), using a Thermo Fisher X Series II (USA) quadrupole mass spectrometer, which has analytical accuracies of <5% and <10% for trace element concentrations greater and less than 10 ppm, respectively.

3.2 U-Pb dating of detrital zircons

Zircon U-Pb dating was performed at the State Key Laboratory of Continental Dynamics at Northwest University, using a laser ablation-ICP-MS (LA-ICP-MS) system including a Micro-Las GeoLas 200M laser ablation system and Agilent 7500a ICP-MS. A laser spot size of 35 μm was used during this process. The zircon U-Pb ages were determined by using the 91500 zircon standard as an external reference. The trace element compositions of the zircons were analyzed using NIST SRM 610 synthetic silicate glass and Si as external and internal standards [32], respectively. Data processing was performed using the ICP-MS-DataCal 9.2 software suite. The method of Andersen (2002) [33] was used for common Pb correction. The concordia and frequency plots of the zircon ages were created using Isoplot 4.15, the ages are used $^{206}Pb/^{238}U$ in interpretations.

4. Results

4.1 Lithological characteristics

The Yimin Formation sandstones are medium-to-fine grained (Fig 2A). Pore and contact cementation are dominant, with some parts showing calcareous cementation. The detrital grains are poorly sorted and rounded. Compositional maturity is low, indicative of short sediment transport distances from the source. Detrital grains account for 85%–90% of the whole-rock composition, while filling materials account for the remaining 10%–15%. Quartz accounts for 30%–40% of the detrital matter. The grains are angular-subangular and range from 0.10 mm to 0.42 mm, a small number exhibit undulatory extinction. Feldspar (mainly plagioclase, Fig 2B), with small amounts of microcline (Fig 2C) and striated feldspar) accounts for 10%–25% of the detrital matter and presented as angular-subangular grains that range from 0.13 mm to 0.48 mm. Clasts (mainly granite fragments (Fig 2D) and small amounts of

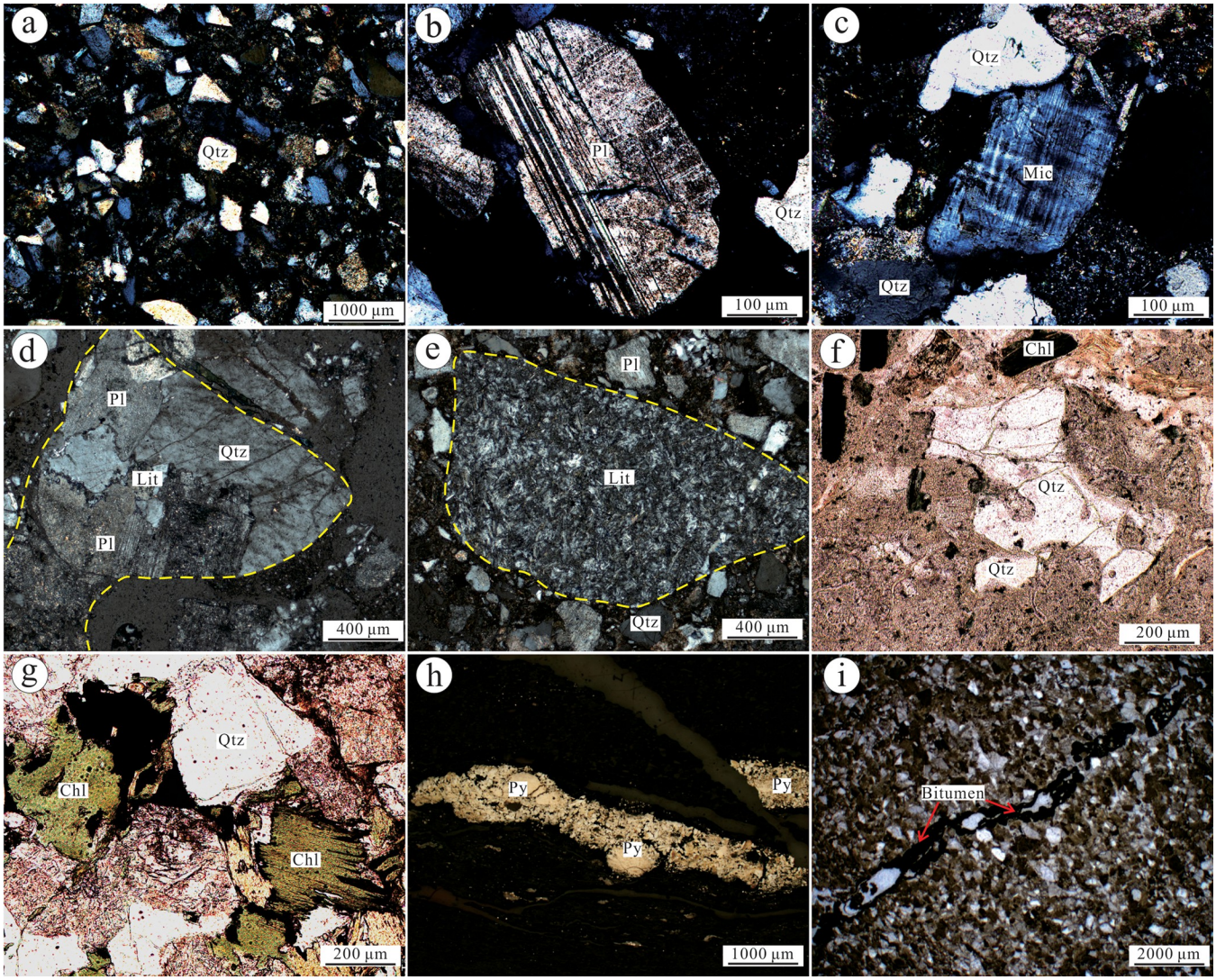

Fig 2. Photographs of thin sections under optical microscopy of the Yimin Formation sandstones. a. Medium-to-fine grained sandstones (cross-polarized). b. Twinned plagioclase crystal (cross-polarized). c. Grid-twinned microcline (cross-polarized). d. Granite fragment (cross-polarized). e. Andesite tuff (cross-polarized). f. Crystal tuff (plane-polarized). g. Chloritized biotite (plane-polarized). h. Pyrite vein (plane-polarized). i. Bitumen vein (plane-polarized).

https://doi.org/10.1371/journal.pone.0309433.g002

andesite (Fig 2E) and crystal tuffs (Fig 2F) account for 20%–50% of the detrital matter and present as angular-subangular grains that range from 0.18 mm to 0.16 mm. Some of these grains had sizes exceeding 1.00 cm. The biotites present as flakes with intense chloritization and account for 2%–4% of the detrital matter (Fig 2G). Some rocks were also interspersed with pyrite (Fig 2H) and bitumen veins (Fig 2I).

4.2 Geochemical characteristics

4.2.1 Major element characteristics. The major element composition of the Yimin Formation sandstones is shown in S1 Table. The Yimin Formation sandstones have SiO_2 contents of 65.88%–74.92%, Al_2O_3 contents of 11.87%–15.98%, $Fe_2O_3{}^T$ contents of 1.45%–6.37%, CaO contents of 0.53%–4.54%, K_2O contents of 2.65%–3.97%, and Na_2O contents of 1.78%–3.67%.

4.2.2 Trace and rare element characteristics. The trace and rare element compositions of the Yimin Formation sandstones are shown in S2 Table. The samples have similar trace element spidergram patterns, characterized by weak enrichment in V, Rb, Co, Y, Nb, and U and weak depletion in Sc, Cr, Ni, Sr, Zr, and Hf relative to concentrations in the upper continental crust (Fig 3).

The total rare earth element (ΣREE), light rare earth element (LREE), and heavy rare earth element (HREE) contents of the samples are 93.1–226.3 ppm, 84.7–205.4 ppm, and 8.4–20.9 ppm, respectively, and LREE/HREE ratios range from 6.4 to 11.9 (S2 Table). Therefore,

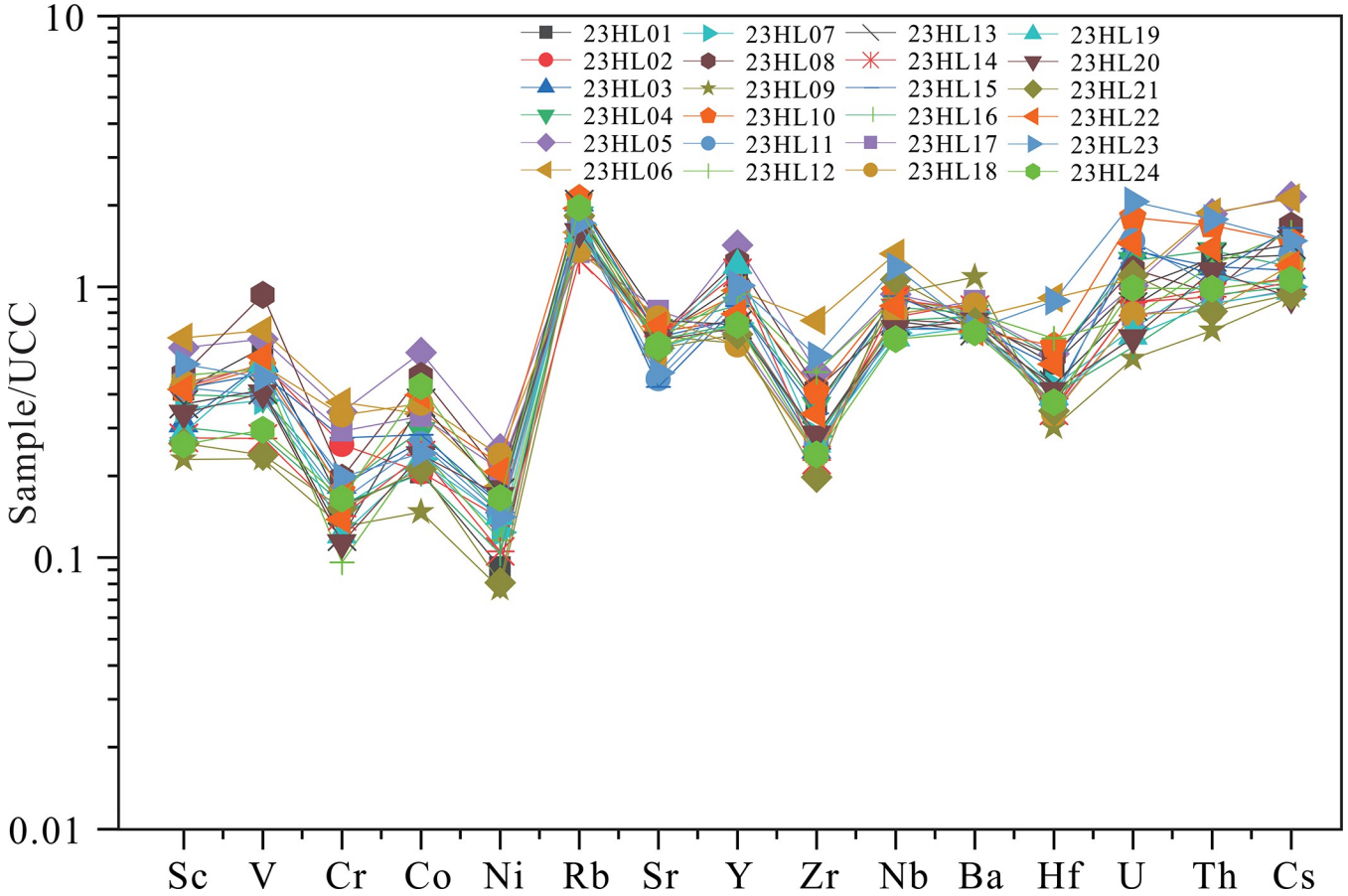

Fig 3. Upper continental crust-normalized trace element spidergram for samples from the Yimin Formation [34].

https://doi.org/10.1371/journal.pone.0309433.g003

the samples show significant LEE/HREE fractionation, with LREE enrichment and HREE depletion. On the chondrite-normalized REE diagram (Fig 4A), these samples have a significant right-inclined pattern and negative Eu anomaly. On the North American shale composite (NASC)-normalized REE diagram, the curve is nearly flat (Fig 4B), suggesting that their REE composition resembles that of North American shales. Hence, the source rocks of the Yimin Formation are derived from the upper continental crust [35].

4.3 U-Pb dating of zircons

Zircons from the Yimin Formation present as euhedral-subhedral grains with long-axis diameters of 100–190 μm and aspect ratios of 1.1–1.8. Most of the grains are angular-subangular (Fig 5), consistent with short transport distances. As the majority of the zircon grains show oscillatory zoning, they are magmatic zircons. As shown in S2 Table, the Th/U ratios of the 23HL02, 23HL07, 23HL11, and 23HL24 samples are 0.4–6.3, 0.1–11.1, 0.1–7.4, and 0.1–3.4, respectively. Since the majority of these Th/U ratios are above 0.4 (Fig 6). Weathering of the parent rock increases Th/U, the Th/U ratios of 0.1–11.1 for detrital zircons, with most samples having values of 0.5–4.0, are consistent with substantial weathering of rocks in the source region [38,39].

After discarding data with concordance <90%, 383 valid age data points were retained for geochronological analyses (S3 Table). In the age concordia diagram (Fig 7) and age spectrum (Fig 8), all four samples plot near the U-Pb concordia line, indicating that the age distributions are consistent with each other (concentrated in the 230–260 Ma range). In particular, the $^{206}Pb/^{238}U$ ages of zircons in the 23HL02, 23HL07, 23HL11, and 23HL24 samples are 230–270, 235–265, 230–260, and 235–260 Ma, respectively.

4.4 Trace element composition of the zircons

The trace element characteristics of detrital zircons can be used to infer the types of rocks in the source region, the mechanism of zircon formation, and the tectonic setting of the source region [39]. As shown in S4 Table, zircons in the 23HL02, 23HL07, 23HL11, and 23HL24 samples have REE contents of 391.6 ppm to 3998.5 ppm, 377.9 ppm to 2219.9 ppm, 367.8ppm to

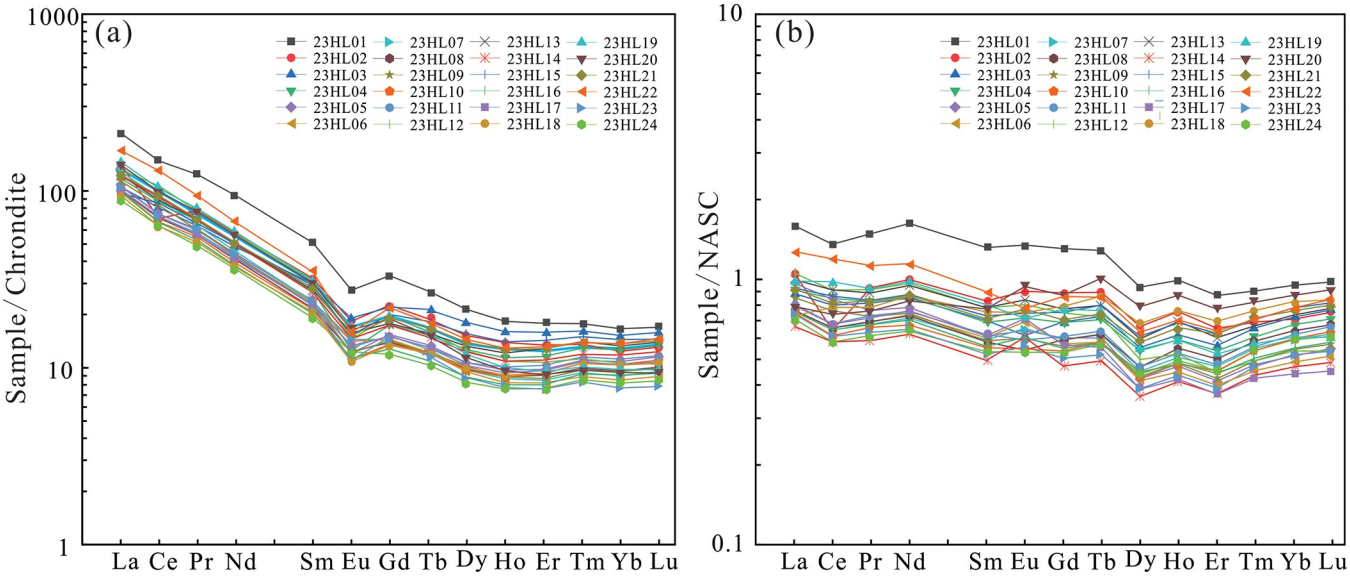

Fig 4. (a) Chondrite-normalized REE diagram [36]. (b) NASC-normalized REE diagram [37].

https://doi.org/10.1371/journal.pone.0309433.g004

Fig 5. Cathodoluminescence images of detrital zircons from the Yimin Formation sandstones, with circles marking laser spot placement and number indicating the obtained $^{206}Pb/^{238}U$ ages.

https://doi.org/10.1371/journal.pone.0309433.g005

3113.36 ppm, and 441.69 ppm to 3418.94 ppm and LREE/HREE ratios of 0.028–0.311, 0.023–0.22, 0.026–0.1, and 0.028–0.302, respectively. Therefore, all four samples show LREE depletion and HREE enrichment. After chondrite normalization (Fig 9), all four samples have similar left-inclined REE fractionation curves, variable negative Eu anomalies, and positive Ce anomalies. Therefore, the detrital zircons in these samples retain the characteristics of magmatic zircons [40].

In the Y-U (Fig 10A) and Nb-Ta (Fig 10B) diagrams, the samples plot in the field of granites. In the Y-Nb/Ta diagram (Fig 10C), the samples mostly plot in the field of overlap between granites, syenite pegmatites, with some mafic rocks and a small number in the field of carbonate rocks. In the Y-Yb/Sm diagram (Fig 10D), the samples mainly plot in the field of overlap between granites, syenite pegmatites, and mafic rocks. Therefore, the parent rocks of the Yimin Formation sandstones are mainly granitoids.

5. Discussion

Trace elements (including REEs) of fine-grained clastic rocks are relatively stable in the later diagenesis and weathering processes, thus making them reliable tools for tracing the provenances and depositional settings [42–45].

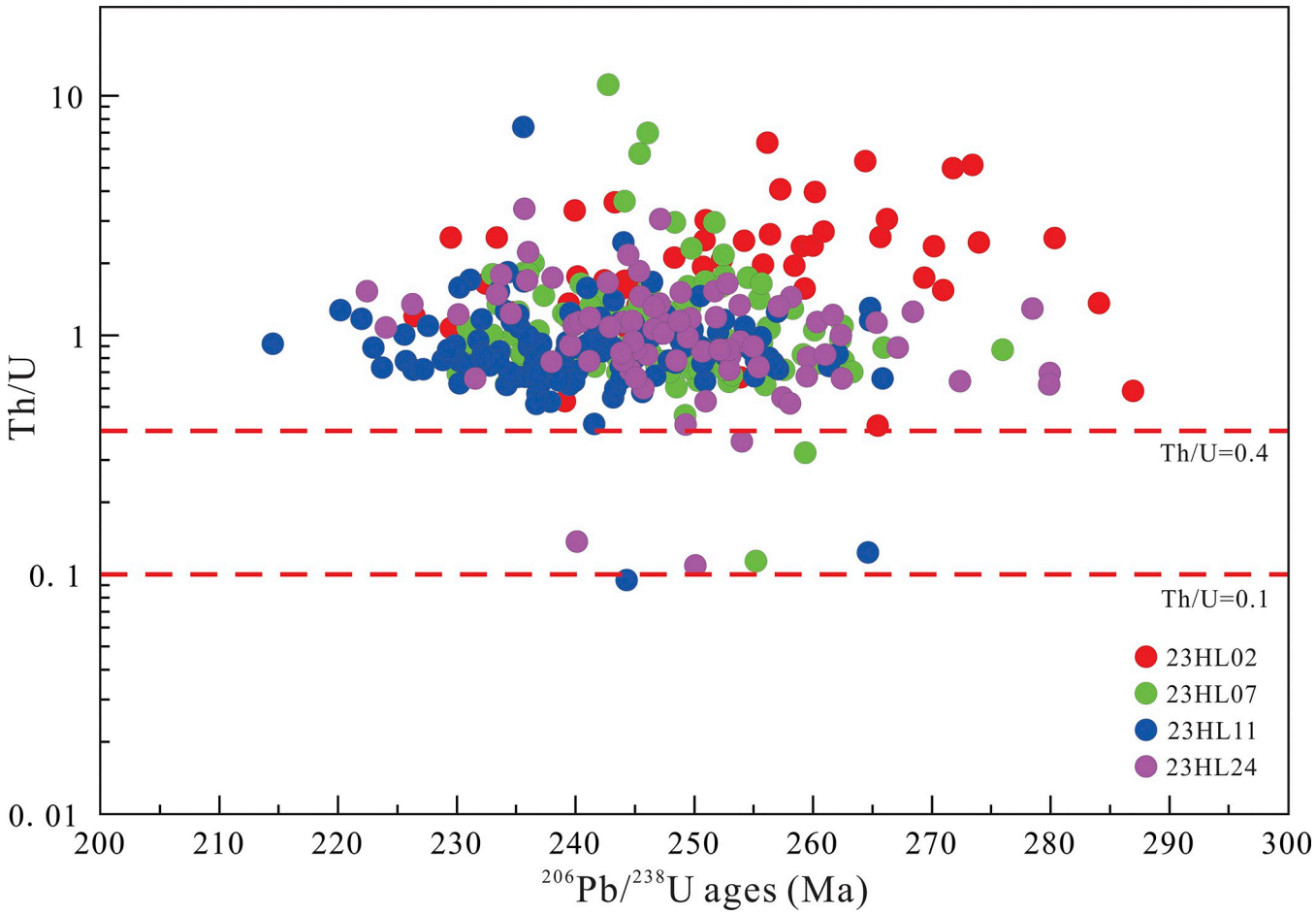

Fig 6. Relationship between zircon ages and Th/U in the Yimin Formation sandstones.

https://doi.org/10.1371/journal.pone.0309433.g006

5.1 Type of parent rocks and tectonic setting of the source

5.1.1 Type of parent rocks. Girty (1996) showed that the Al_2O_3/TiO_2 ratio is an effective parameter for discriminating the provenance of sandstones [46], where sandstones derived from mafic rocks have Al_2O_3/TiO_2 ratios less than 8 and sandstones derived from intermediate and felsic igneous rocks have Al_2O_3/TiO_2 ratios of 8–21 and >21, respectively. As the Yimin Formation sandstones have Al_2O_3/TiO_2 ratios of 18.43–55.34, their parent rocks are felsic igneous rocks. In the TiO_2-Al_2O_3 diagram (Fig 11A), the samples largely plot in the field of granites and granodiorites. In the F_2-F_1 diagram (Fig 11B), all of the sample plot in the field of felsic igneous rocks. In the K_2O-Rb diagram (Fig 11C), they plot in the field of intermediate-to-acidic rocks. In the TiO_2-Ni diagram (Fig 11D), they plot within and around the field of acidic rocks.

In the Co/Th-La/Sc diagram (Fig 12A), all samples plot in the field of felsic igneous rocks and granites. In the Th/Sc-Cr/Th (Fig 12B) and Th/Sc-Cr/Th diagrams (Fig 12C), they plot between felsic igneous rocks and granites. In the La/Th-La/Yb diagram (Fig 12D), all samples plot near the averages of the upper continental crust. In the La-Th-Sc (Fig 13A), Th-Hf-Co (Fig 13B), and V-Ni-Th×10 diagrams (Fig 13C), all the Yimin Formation samples plot in the field of granites and felsic igneous rocks. Therefore, the Yimin Formation sandstones were derived from felsic igneous rocks in the upper crust.

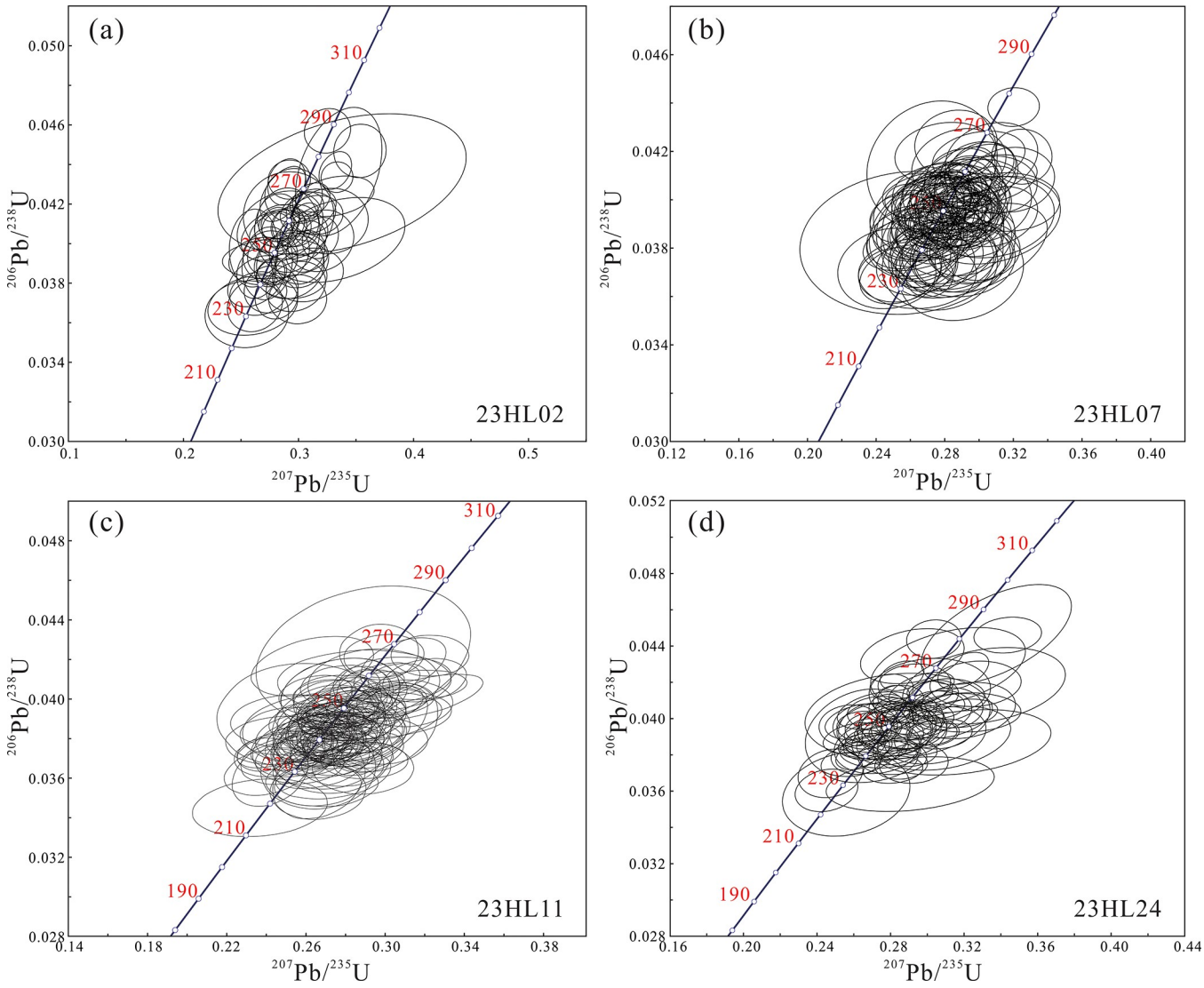

Fig 7. Concordia diagram of detrital zircon LA-ICP-MS U-Pb ages.

https://doi.org/10.1371/journal.pone.0309433.g007

5.1.2 Tectonic setting of the source region. Basin structures can be classified into one of four types according to their crustal characteristics: oceanic island arcs, continental island arcs, active continental margins (ACMs), and passive margins (PMs). The tectonic setting of a source region can be inferred using the presence of stable oxides like Al_2O_3, SiO_2, TiO_2, $Fe_2O_3^T$, and MgO. In the $K_2O/(Na_2O+CaO)$-SiO_2/Al_2O_3 (Fig 14A) and K_2O/Na_2O-SiO_2 diagrams (Fig 14B), the samples from the Yimin Formation mostly plot in the field of ACMs. In the TiO_2-($Fe_2O_3^T$+MgO) (Fig 14C) and Al_2O_3/SiO_2-($Fe_2O_3^T$+MgO) diagrams (Fig 14D), these samples largely plot in the field of ACMs, with a few plotting outside but near this field. In the La-Th-Sc diagram (Fig 15A), all the Yimin Formation samples plot in the field of ACMs and PMs. In the Th-Sc-Zr/10 (Fig 15B) and Th-Sc-Zr/10 diagrams (Fig 15C), all of the samples plot in the field of ACMs.

The Hailar Basin was affected by the southward subduction of the Mongolia-Okhotsk Plate, resulting in extensive volcanic activity and the formation of a large number of Late Paleozoic granites in Manzhouli, southern Hailar Basin. The Late Paleozoic granites in the western part

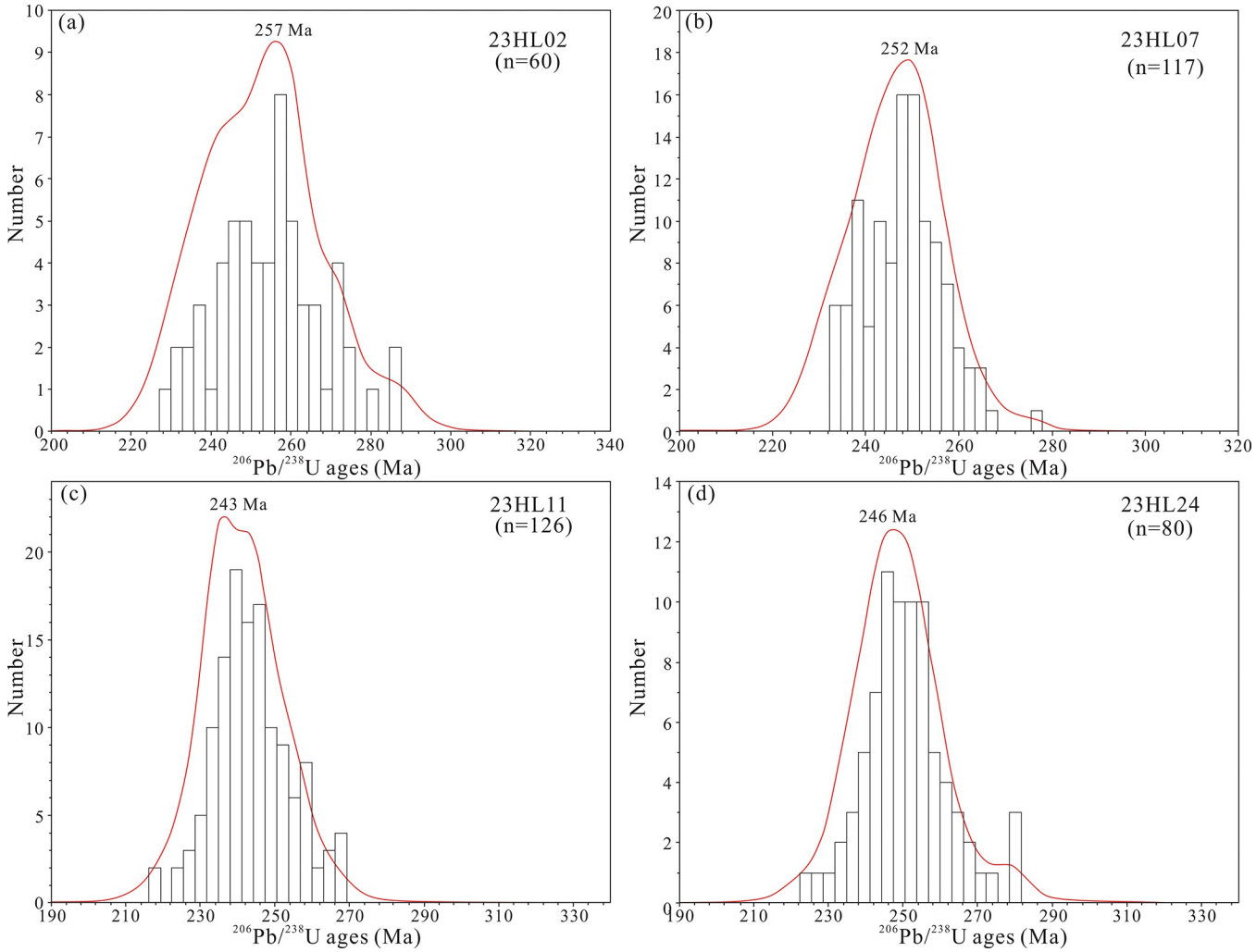

Fig 8. Age spectrum of detrital zircons from the Yimin Formation sandstones.

https://doi.org/10.1371/journal.pone.0309433.g008

of the Kelulun Depression have undergone weathering, erosion, and transportation into the basin [60]. Because the composition and geochemical characteristics of clastic rocks are influenced mainly by the tectonic background of the source area, the complex tectonic background identified by the geochemical feature analysis does not represent the tectonic environment during the formation of detrital rocks but rather reveals the tectonic environment during the formation of the corresponding detrital source rocks. These findings suggest that the tectonic setting of the source region of the Yimin Formation sandstones was an ACM.

5.2 Paleoweathering characteristics of the source region

The chemical composition of a sandstone is influenced by weathering, transport, and sedimentation, as well as post-diagenetic processes. As weathering increases, sandstone shows the loss of mobile oxides, increase in stable oxides, and total element loss [61,62]. Therefore, the oxide content is an indicator of the degree of weathering of parent rocks in the source region [63,64].

Intense weathering of the parent rocks is supported by analyses of the Chemical Index of We-athering (CIW = $100Al_2O_3/(CaO^*+Na_2O+Al_2O_3)$, Chemical Index of Alteration (CIA = $100Al_2O_3/(Al_2O_3+CaO^*+Na_2O+K_2O)$, and Index of Chemical Variability (ICV =

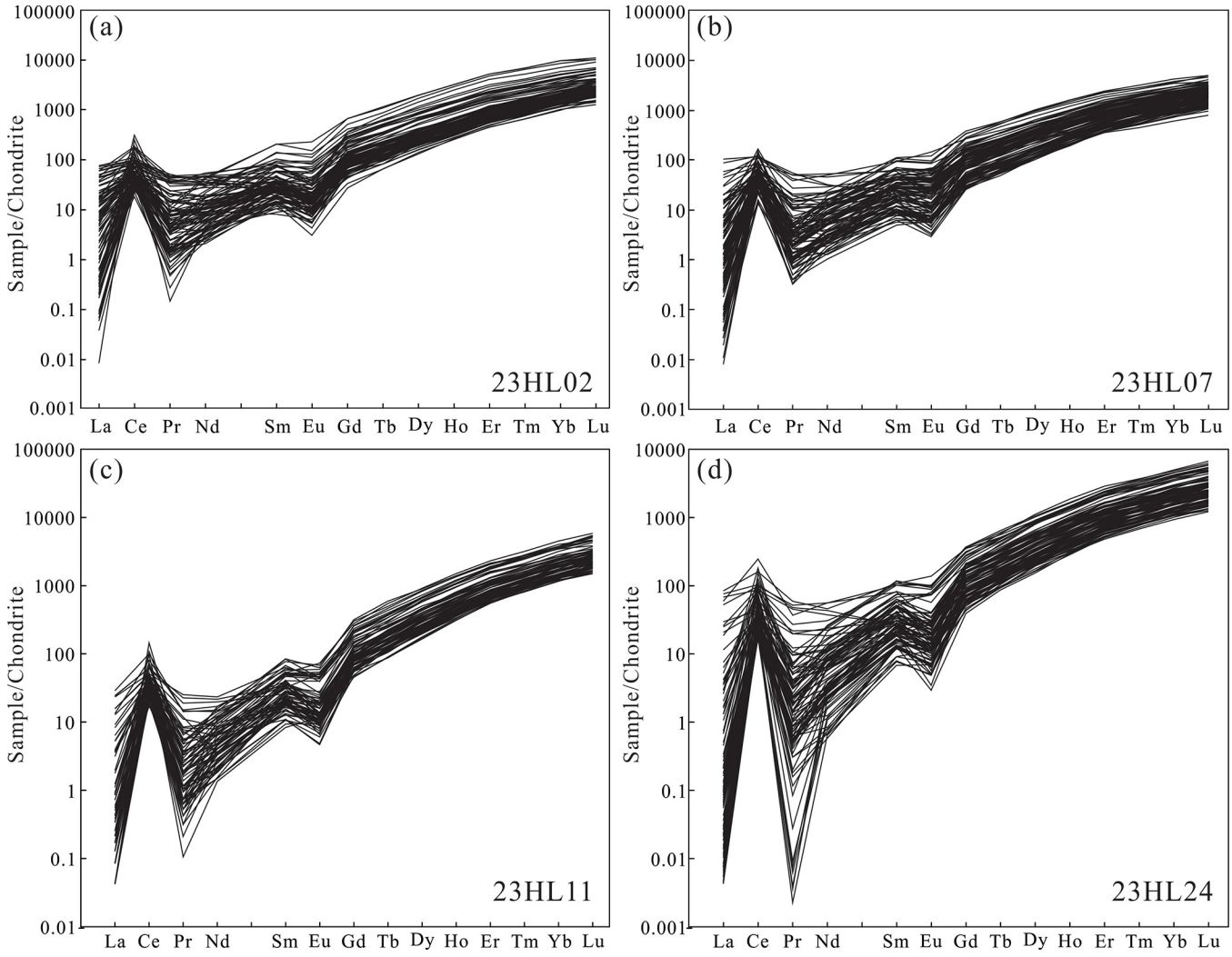

Fig 9. Chondrite-normalized REE fractionation curves of detrital zircons from the Yimin Formation sandstones [36].

https://doi.org/10.1371/journal.pone.0309433.g009

($Fe_2O_3^T$+Na_2O+K_2O+CaO+MgO+TiO_2)/Al_2O_3). Briefly, CIA values of 50–60, 60–80, and 80–100 are indicative of low, moderate, and intense chemical weathering [65], respectively. ICV < 1 and ICV > 1 indicate intense and relatively low weathering [66–68], respectively. CIW values of 50–60 indicate fresh rocks, and CIW > 70 indicates intense weathering [69]. The Yimin Formation sandstones have CIA values of 42.18–65.39 and CIW values of 48.50–76.26, indicating that their parent rocks were moderately to st-rongly weathered. Observed ICV values of 0.84–1.66 (mostly 0.85–1.0) indicate that the rocks in

the source region have been strongly weathered. In the A-CN-K diagram (Fig 16A), the CIA valu-es of the Yimin Formation sandstones are largely 55–70, indicating that the felsic rocks in their so-urce region have undergone moderate-to-strong weathering. The CIA-ICV diagram (Fig 16B) ind-icate that the Yimin Formation sandstones are compositionally immature, which is indicative of a moderately high degree of weathering in the parent rocks. In summary, the source region of the Yi-min Formation sandstones has undergone moderately strong weathering, promoting erosion of the parent rock and thus providing an ample supply of detrital matter for the study area.

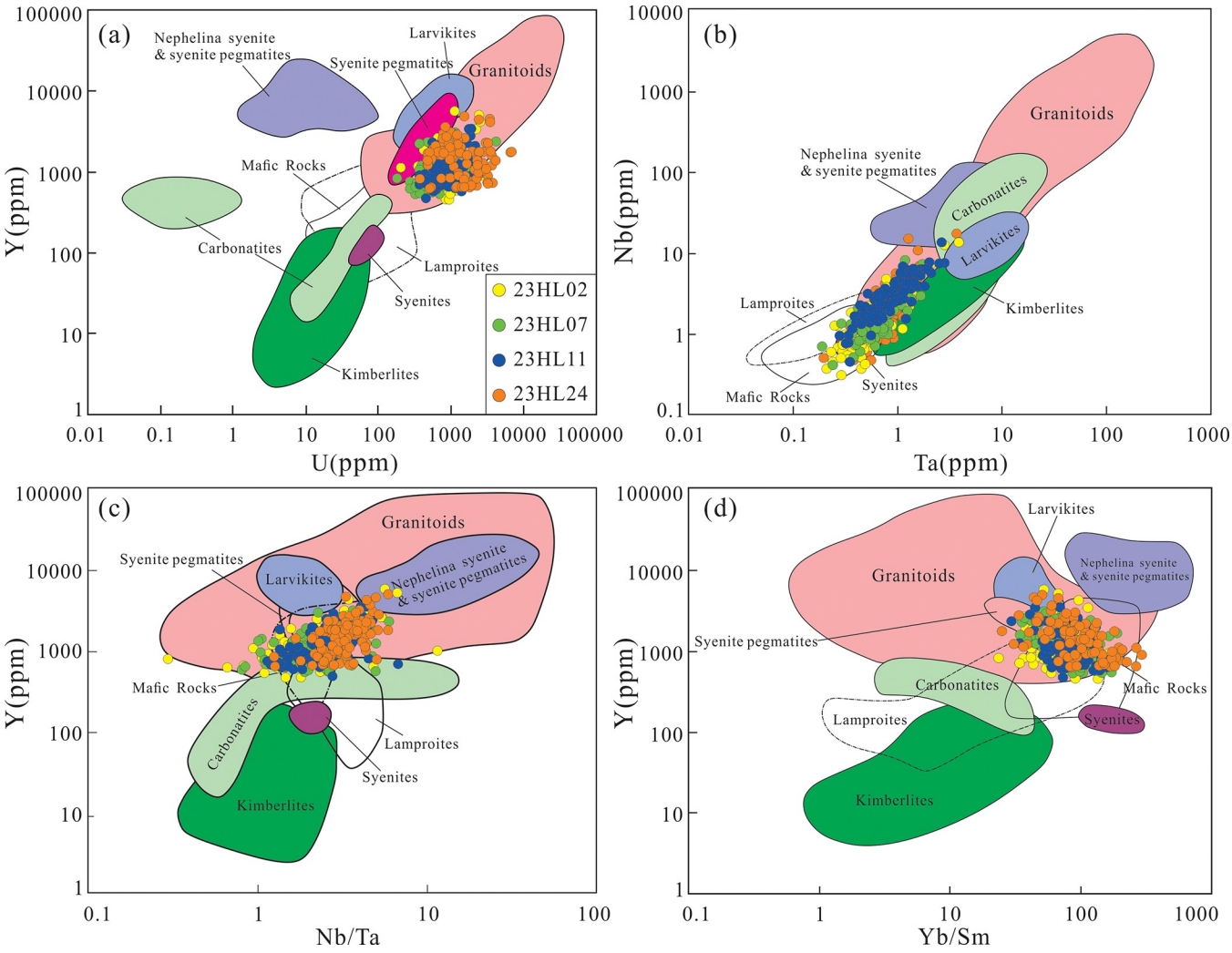

Fig 10. Zircon trace element discrimination diagrams for the Yimin Formation sandstones [41]. a. Y-U diagram. b. Nb-Ta diagram. c. Y-Nb/Ta diagram. d. Y-Yb/Sm diagram.

https://doi.org/10.1371/journal.pone.0309433.g010

5.3 Provenance analysis

5.3.1 Constraints on provenance from regional sedimentology. The deposition of the Yimin Formation occurred in the tectonic transition between rifting and subsidence, which shrank lake basins and formed a sedimentary system consisting of fan-delta plains, fan-delta fronts, and pre-fan deltas (Fig 17) [71,72]. The Adunchulu Uplift provided abundant matter to this steep monocline, promoting the formation of fan deltas inside the depression. Furthermore, due to the steep terrain, weathering and erosion on the western side of the source region created vast quantities of detrital matter, which were washed by floods into the basin and deposited in saddle landforms. Large near-source fan deltas filled with coarse clastic and sandy conglomerates were thus formed.

After the Yimin Formation was deposited, the terrain gradually became flattened, which decreased the difference in height between the depression and its surrounding uplifts. Consequently, the base of the alluvial fans and middle-fan subfacies on the western side were denuded, and the landscape inside the depression became dominated by fan-delta plains and

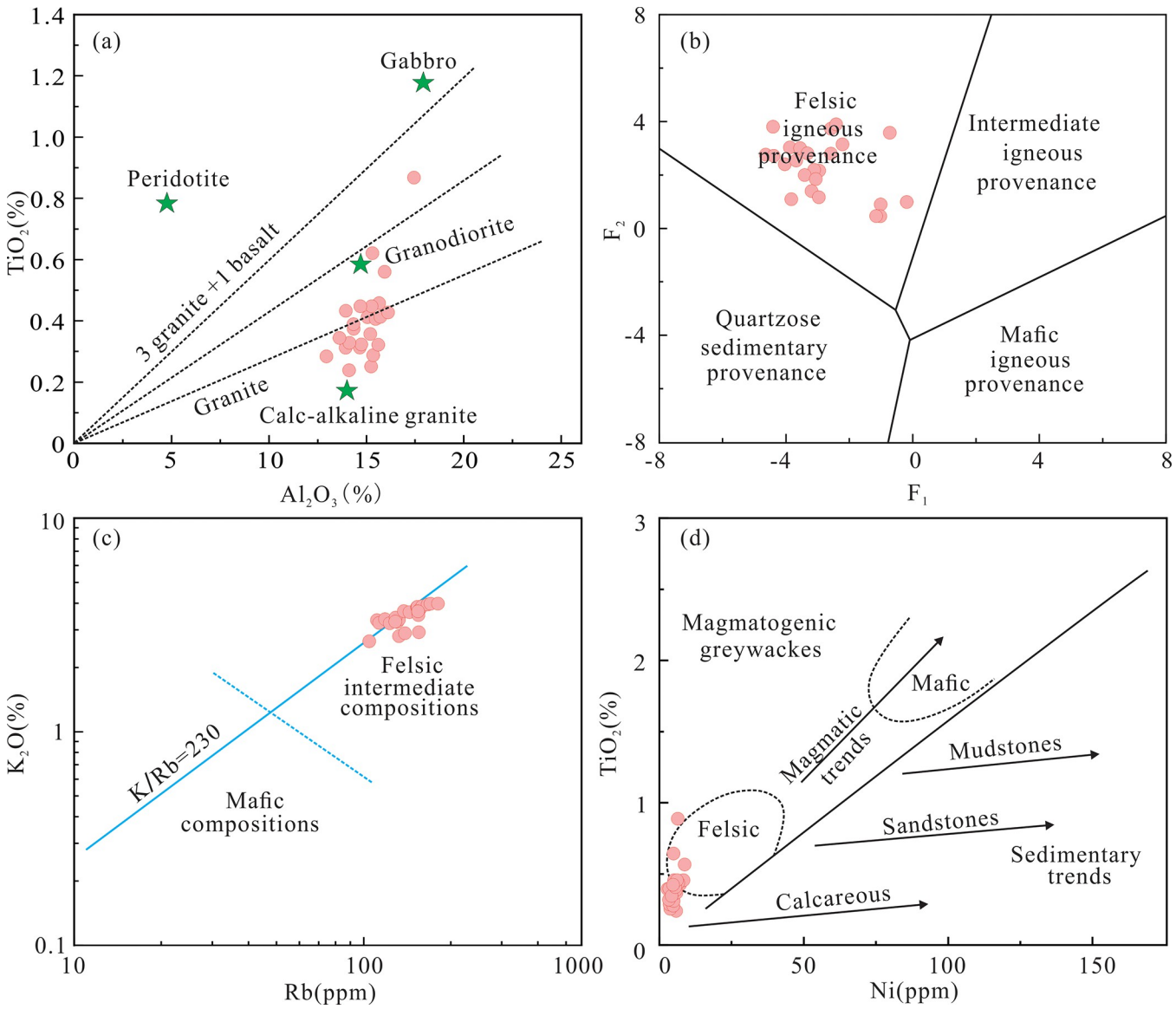

Fig 11. Major element discrimination diagrams for the parent rocks of the Yimin Formation sandstones. a. TiO_2-Al_2O_3 diagram [47]. b. F_2-F_1 diagram [48]. c. K_2O-Rb diagram [49]. d. TiO_2-Ni diagram [50].

https://doi.org/10.1371/journal.pone.0309433.g011

fronts. The fan-delta plains spread along the depression in the NE direction. Their sediments are coarse and compositionally immature clastic and sandy conglomerates dominated by granite and brown-yellow or brick-red colors. Fan-delta fronts developed in the central and western parts of the depression, and their sediments are grey-colored medium- and fine-grained sandstones, with predominantly quartz and feldspar clasts. Organic clasts like detrital coal are also common. The most common facies here are underwater distributary channel, interdistributary bay, and estuary bar microfacies. Pre-fan deltas developed on the southern and northern ends of the depression, and their sediments are grey and dark-grey mudstones and siltstones intercalated with large quantities of detrital coal [73]. In summary, the sedimentary facies and sandbody distribution indicate that the materials of the Yimin Formation were derived from the Adunchulu Uplift at the western side of the Kelulun Depression.

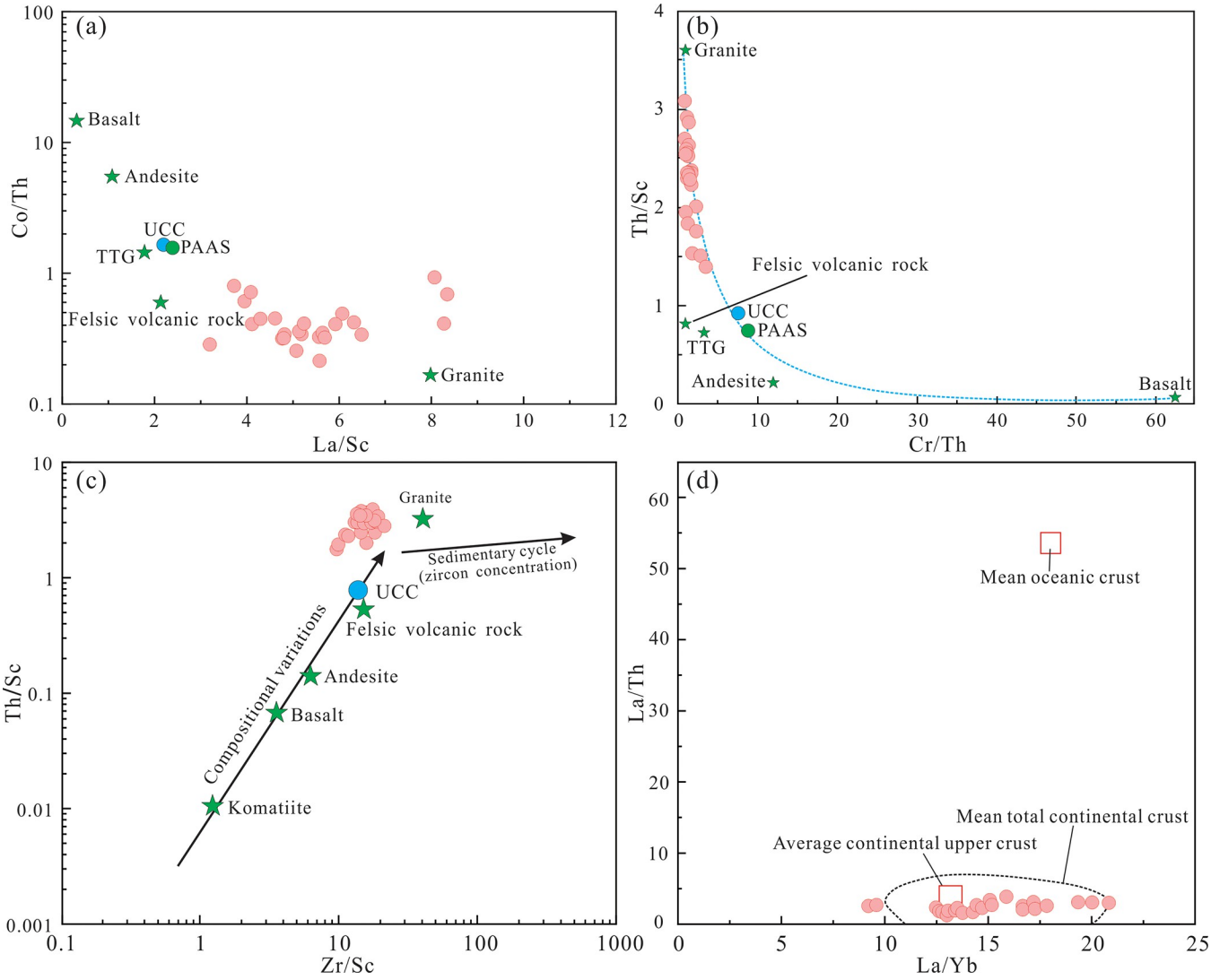

Fig 12. Trace element discrimination diagrams for the parent rocks of the Yimin Formation sandstones. a. Co/Th-La/Sc diagram [51]. b. Th/Sc- Cr/Th diagram [52]. c. Th/Sc-Zr/Sc diagram [53]. d. La/Th-La/Yb diagram [54]. UCC: Upper continental crust. PAAS: Post-archean Australian shale. TTG: Trondhjemite-tonalite-granodiorite.

https://doi.org/10.1371/journal.pone.0309433.g012

5.3.2 Constraints on provenance from zircon U-Pb ages. Age dating of geological bodies around the Kelulun Depression, i.e., the Adunchulu Uplift, Bayang Shan, and Erentaoleigai, revealed the spatiotemporal distribution of material sources around the Kelulun Depression (Fig 1c). The Hailar Basin has undergone many periods of granitic magmatism throughout its geological evolution, which formed acidic igneous rocks of varying ages in the southern part of Manzhouli [74,75]. Permian granites (280–335 Ma) mainly outcrop in the eastern part of the depression, around Erentaoleigai [76]. Most of the Middle-Late Triassic alkali feldspar granites (205–260 Ma) outcrop at the western part of the depression [77,78], at the Adunchulu Uplift. A few outcrops have also been observed at Chagantaoleigai, Bayan Shan, Jiawula-Chaganbulagen, and Erentaoleigai. Early Jurassic monzogranites and granite porphyries (175–185 Ma) mainly outcrop in the northern part of the depression [78,79], at Wunugetushan and Dashimo, whereas Late Jurassic–Early Cretaceous biotite granites and granite porphyries (125–160 Ma) are mainly located at the Adunchulu Uplift [80,81]. Mesozoic volcanism in southern

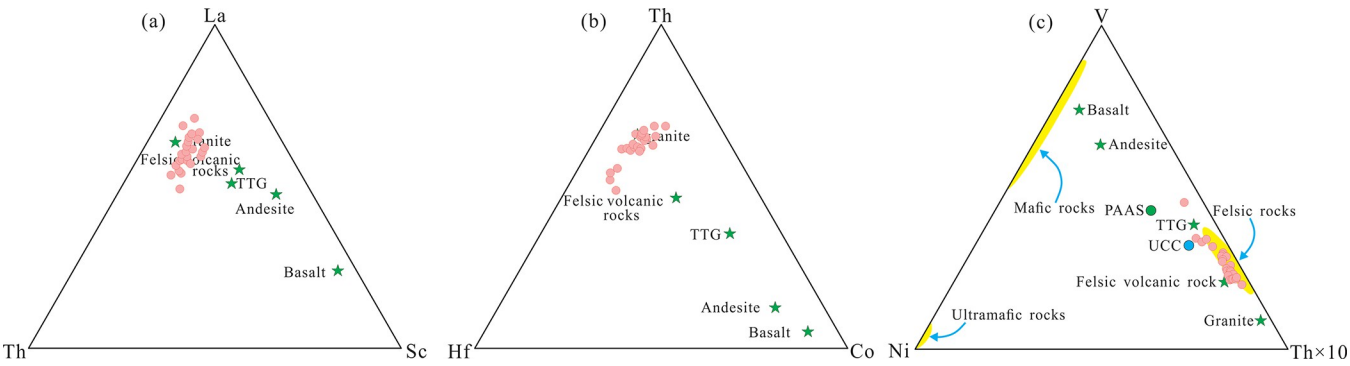

Fig 13. Triangular trace-element discrimination diagrams for the parent rocks of the Yimin Formation sandstones. a. La-Th-Sc diagram [55], b. Th-Hf-Co diagram [34], c. V-Ni-Th×10 diagram [52]. UCC: Upper continental crust. TTG: Trondhjemite-tonalite-granodiorite. PAAS: Post-archean Australian shale.

https://doi.org/10.1371/journal.pone.0309433.g013

Manzhouli started in the Middle-Late Jurassic and persisted until the Early Cretaceous, and its effects are most pronounced on the two sides of the Mongol-Okhotsk suture. Rhyolites, andesites, and olivine basalts with ages of 120–165 Ma were formed by this volcanism [82], and they mainly outcrop in the southern and northern parts of the depression (the Hanwula Uplift and Bayang Shan, respectively).

The ages of the detrital zircons found in Yimin Formation sandstones range from 215 Ma to 287 Ma and are most commonly distributed in the range of 230–260 Ma. Therefore, the geological ages of the sources of these sandstones correspond to the Early-Middle Triassic and are consistent with the age peak of Triassic granites in the Adunchulu Uplift (western part of the depression) (Fig 18). In view of the lithologic, geochemical, and chronological evidence, we conclude that the detrital matter in the Yimin Formation was largely derived from Triassic granites in the Adunchulu Uplift. During the Triassic, large quantities of granite formed in southern Manzhouli due to the southward subduction of the Mongol-Okhotsk oceanic plate [83–85]. These granites subsequently underwent uplifting and denudation since the Late Cretaceous, which supplied ample quantities of detrital matter to the Kelulun Depression. Sourcing of Triassic granites related to an old subduction zone explains the ACM geochemical characteristics of the studied sandstones.

5.4 Source of uranium

Sandstone uranium deposits are derived from uranium-rich rocks and sedimentary layers in the erosion source-area as well as the ore-bearing stratum itself [86]. The scale of uranium mineralization is in part determined by the uranium content and outcropping area of the parent rock. If the ore-bearing strata receive large quantities of detrital uranium during sedimentation and diagenesis, their capacity to act as a source of uranium will be greatly enhanced. This also establishes a foundation for large-scale uranium mineralization [87].

In the Kelulun Depression, Late Paleozoic granites have uranium contents of 2.7 ppm to 22.3 ppm, while Mesozoic granites have uranium contents of 2.8 ppm to 5.4 ppm [88]. These uranium levels far exceed the average of the upper continental crust (2.80 ppm), indicating that the area is a good source [34]. Late Paleozoic granites in this area have Th/U ratios of 3.79–9.29 (6.33 on average) and uranium mobilization rates of 65%–75%, whereas Mesozoic granites have Th/U ratios of 4.23–8.16 (5.24 on average) and uranium mobilization rates of 55%–90%. These (high) Th/U ratios and uranium mobilization rates indicate that vast amounts of uranium may have migrated out of these rocks [89,90]. The uranium contents of the Yimin Formation strata range from 1.48 ppm to 5.50 ppm [71], and these estimates are

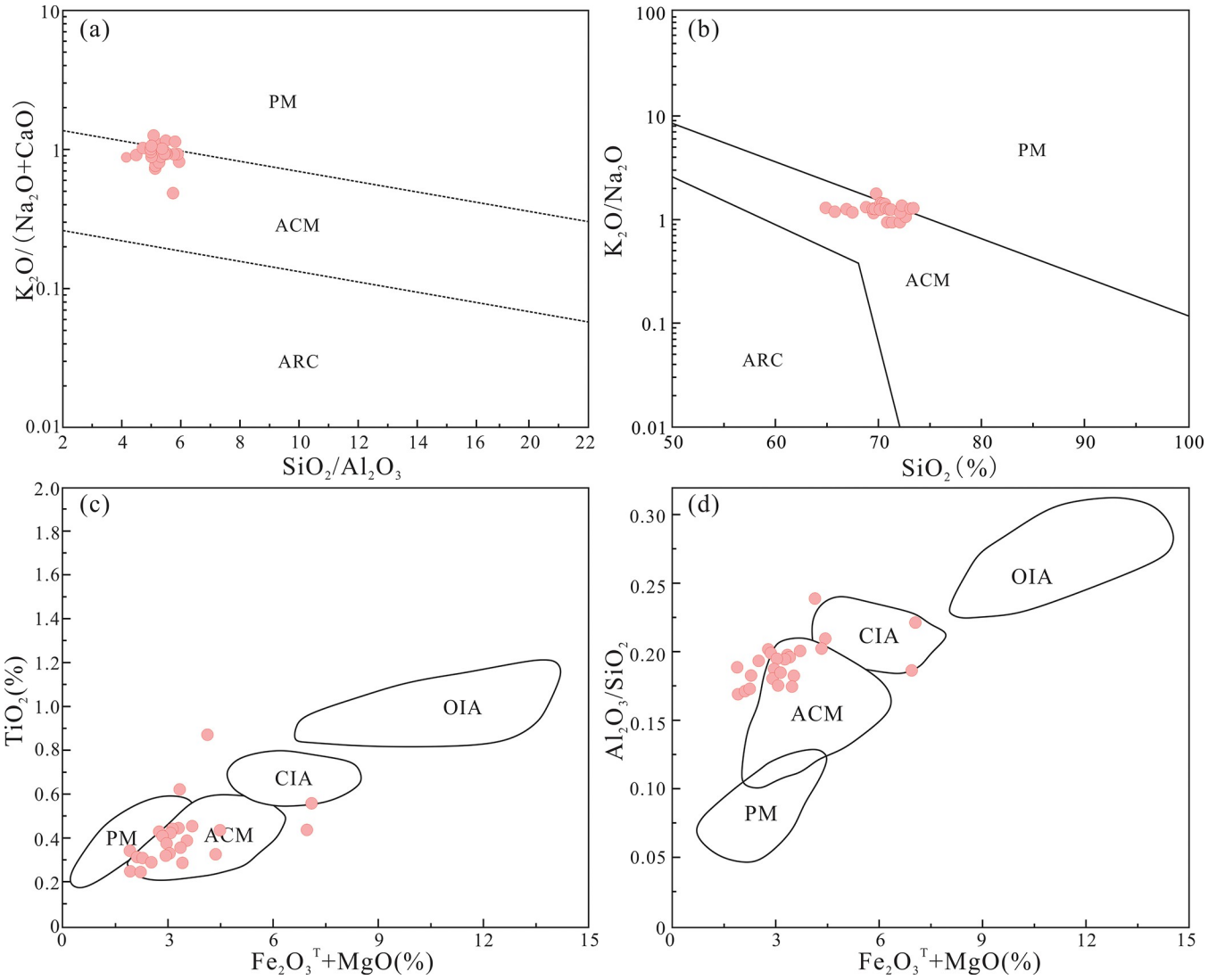

Fig 14. Major element discrimination diagrams for the tectonic setting of the Yimin Formation sandstones. a. $K_2O/(Na_2O+CaO)$-SiO_2/Al_2O_3 diagram [56]. b. K_2O/Na_2O-SiO_2 diagram [57]. c. TiO_2-($Fe_2O_3^T$+MgO) diagram [58]. d. Al_2O_3/SiO_2-($Fe_2O_3^T$+MgO) diagram [59]. PM: Passive continental margin. ACM: Active continental margin. ARC: Oceanic island arc margin. OIA: Oceanic island arc. CIA: Continental island arc.

https://doi.org/10.1371/journal.pone.0309433.g014

higher than the global average for sandstones (0.45 ppm). Therefore, uranium-containing clasts may have migrated with subsurface waters into the depression during the weathering of uranium-rich granites in the erosion source area, which resulted in high uranium concentrations within the sandbody of the Yimin Formation. In addition, multiple rounds of fluid-induce dissolution during the diagenetic processes of the Yimin Formation created substantial secondary porosity. This increased the porosity of the sandbody and the interconnectivity of its pores, thus creating channels that facilitated the migration of uranium-containing oxygenated water. The dissolving fluids in the study area consist mainly of atmospheric precipitation and infiltrating waters, in the erosion source area, the bedrock fissure waters, porewaters, and groundwater have uranium concentrations of 14.4 ppm to 225 ppm, 130 ppm to 204 ppm, and 0.78 ppm to 243 ppm [13,15], respectively. Therefore, the atmospheric precipitation and infiltrating waters leached uranium from the parent rocks to create uranium- and oxygen-rich

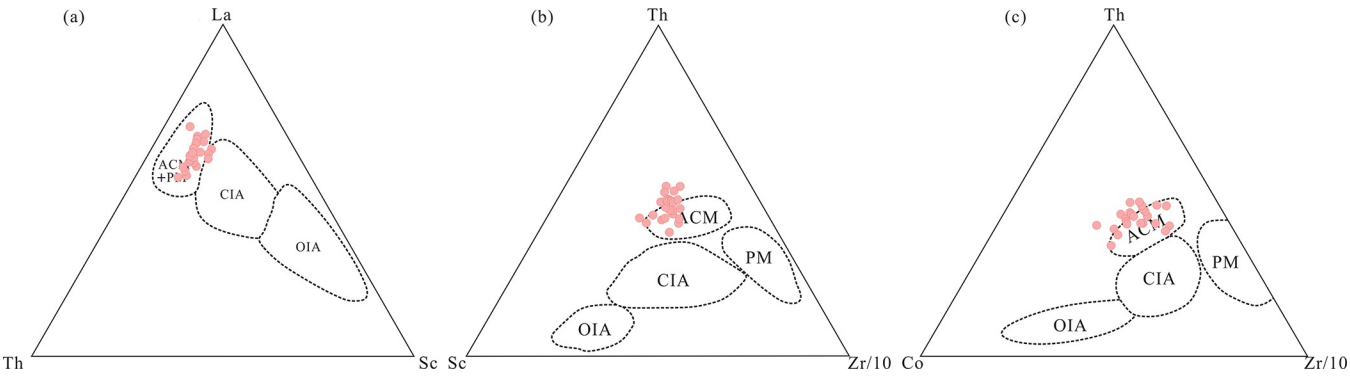

Fig 15. Trace element discrimination diagrams for the tectonic setting of the Yimin Formation sandstones. a. La-Th-Sc diagram, b. Th-Sc-Zr/10 diagram, c. Th-Co-Zr/10 diagram [58]. PM: Passive continental margin. ACM: Active continental margin. OIA: Oceanic island arc. CIA: Continental island arc.

https://doi.org/10.1371/journal.pone.0309433.g015

fluids, which migrated along the margins of the erosion source area into the Kelulun Depression. This created a stable and abundant source of uranium for the formation of sandstone uranium deposits in the Yimin Formation.

5.5 Constraints on uranium mineralization by the tectonic evolution of the source region

Beginning of rifting in the Late Jurassic: The Hailar Basin as a whole is a continental rift basin that has undergone multi-stage tectonic activities [60,91]. Before the Late Jurassic, the Hailar Basin was affected by the southward subduction of the Mongolia-Okhotsk Plate, resulting in extensive volcanic activity and the formation of a large number of Late Paleozoic granites in Manzhouli, southern Hailar Basin [92], which provided a rich material basis for the formation

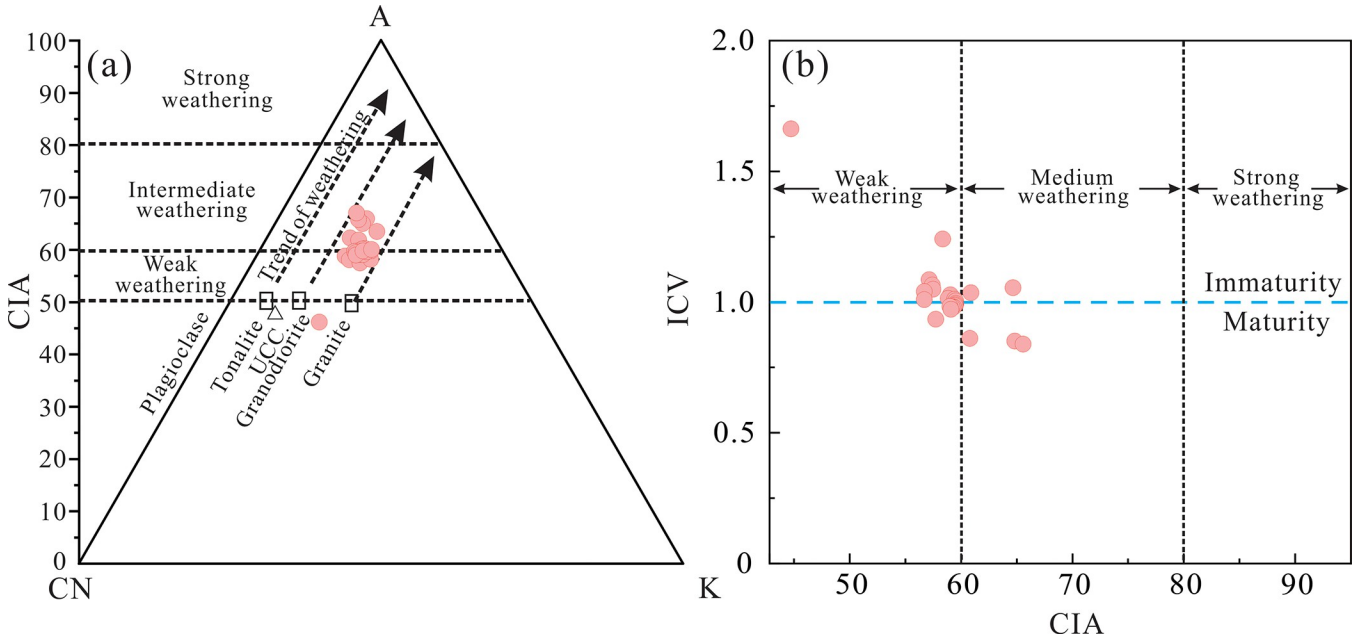

Fig 16. Discrimination diagrams for the paleoweathering characteristics of the source region of the Yimin Formation sandstones. a. A-CN-K diagram [70]. b. ICV-CIA diagram [63]. UCC: Upper continental crust.

https://doi.org/10.1371/journal.pone.0309433.g016

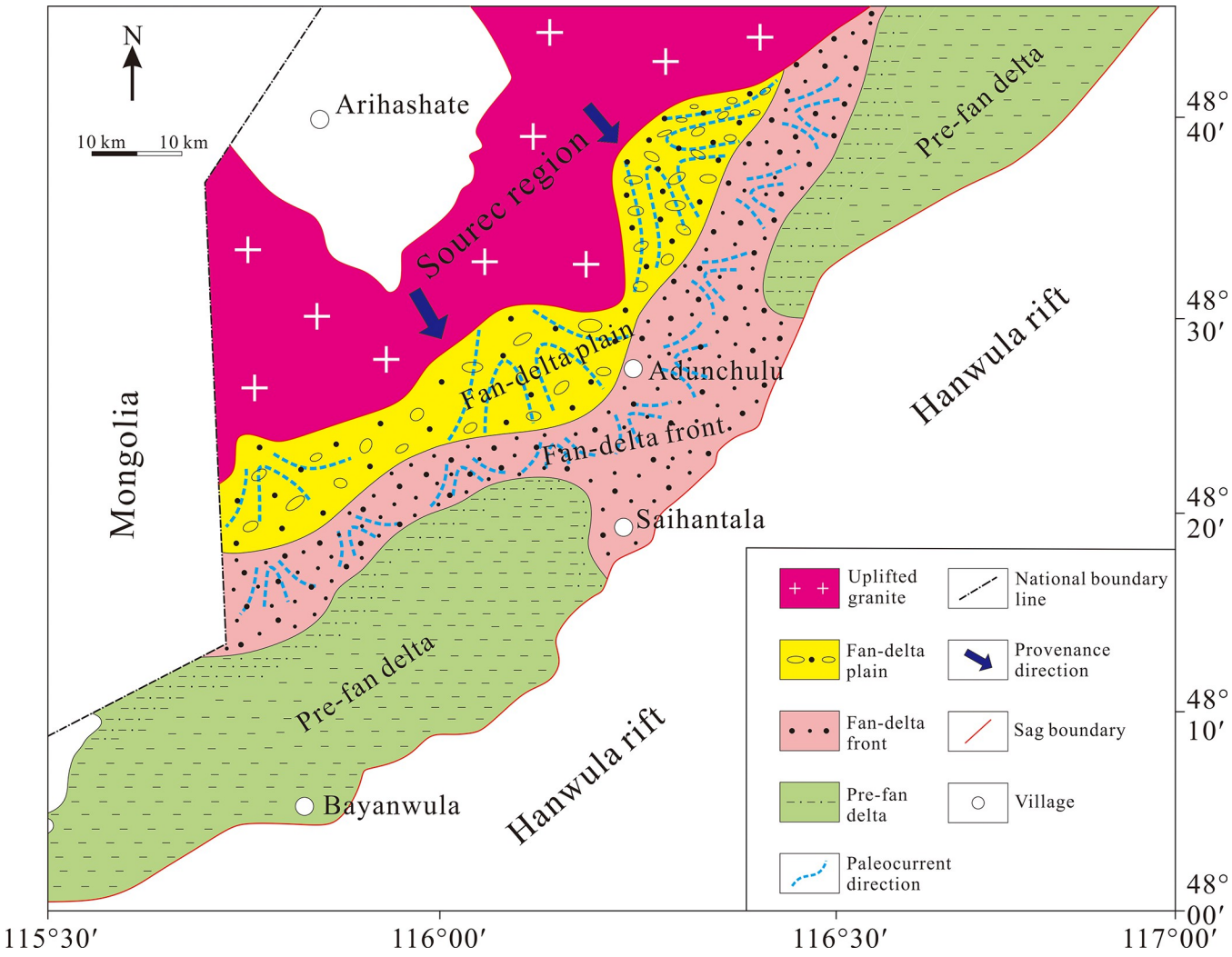

Fig 17. Sedimentary facies map of the Yimin Formation in the Kelulun Depression [19]. Republished from [Zhou W.B, Zhang R, Liu T, Mu H.Q, Zhao Z. W, Huang X. Metallogenic Geological Features and Prospective Study for Sandstone-type Uranium Deposit in Bel-Ulson Depression 2020; 53(03), 201–209.] under a CC BY license, with permission from [Northwestern Geology], original copyright [2020].

https://doi.org/10.1371/journal.pone.0309433.g017

of mineralized strata and uranium source supply. Since the Late Jurassic, the upper crust was transformed from a compressional system to a tensional background due to the hot rise of the deep mantle, and the Hailar Basin was formed under the extensional background.

Pull-apart stage in the Early Cretaceous: Due to deep mantle upwelling, a change in the stress state of the upper crust from a compressional to extensional regime marked the beginning of an extensional pull-apart stage [91–93]. During this period, tectonic activity was extremely intense in the study area, resulting in vast differences in altitude between the basin and its surrounding uplifts. Many alluvial fans and fan-deltas formed as well as semi-deep and deep lake sediments, with only a few small sandbodies. These sandbodies did not undergo large-scale uplifting and denudation, preventing post-diagenetic oxidation from occurring on a large scale. These conditions are generally not conducive to the development of uranium deposits.

Basin shrinkage in the middle-to-late Early Cretaceous: As the study area transitioned from rifting to subsidence, the rift basin also shrank, and the tectonic activity in the area started to

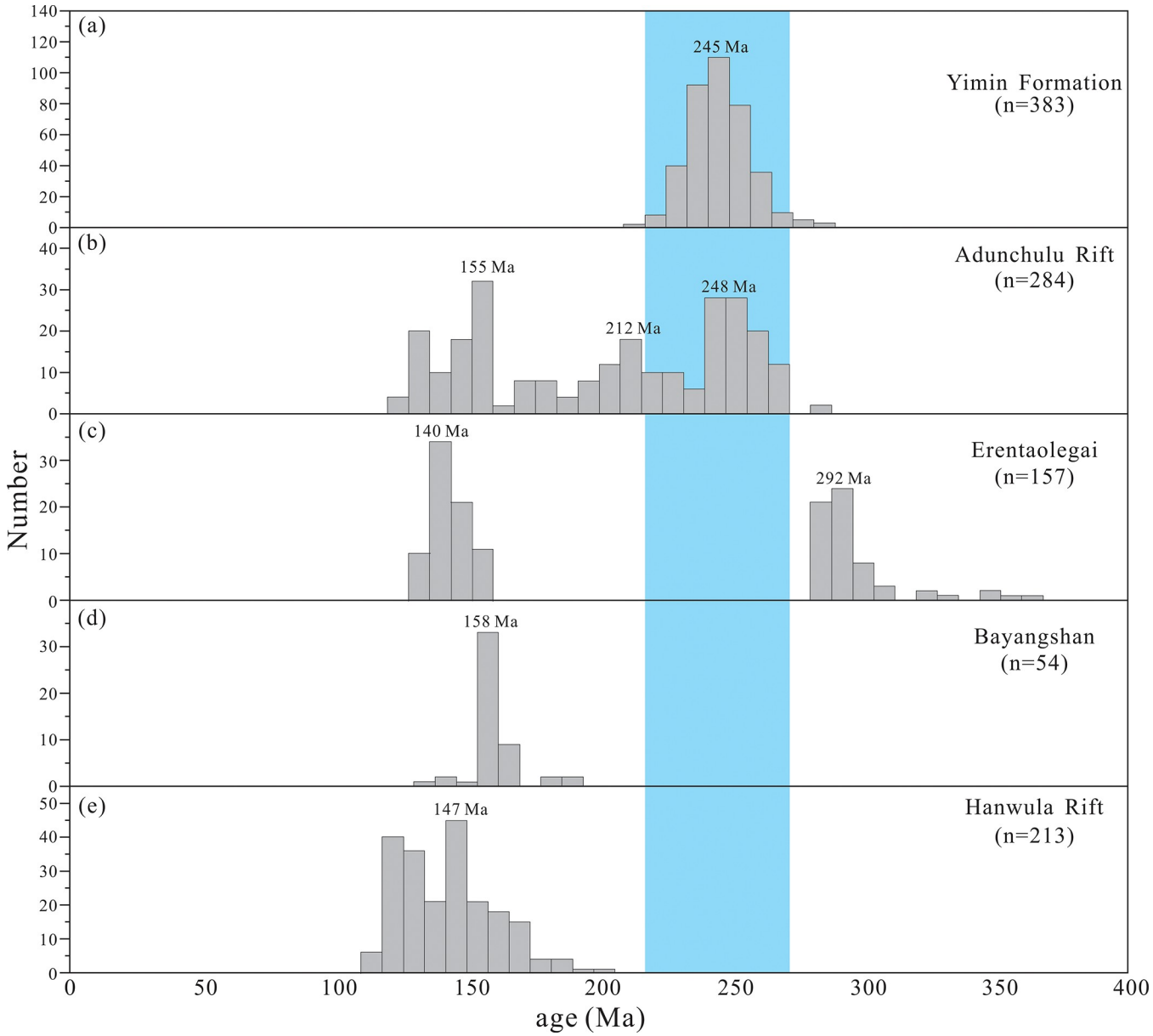

Fig 18. U-Pb age spectra of detrital zircons from the Yimin Formation sandstones and geological bodies around the Kelulun Depression [76–85]. (n represents the number of zircons).

https://doi.org/10.1371/journal.pone.0309433.g018

subside [94–96]. The altitude disparity between the basin and its surrounding mountains started to decrease. In this stage, the Yimin Formation was largely comprised of grey-colored coal-bearing detrital matter. As such, its sandbody was loosely packed and large, with excellent lateral connectivity. Furthermore, it had a stable roof and floor made of impermeable shale. These conditions were conducive for the migration of oxygenated uranium-containing waters and the formation of uranium deposits. In addition, the prevailing paleoclimate during the deposition of the Yimin Formation was wet and warm, resulting in large quantities of plant detritus, detrital coal, and pyrite to mix with the grey sandbody [19,31]. Consequently, this sandbody has a high native reducing capacity and is also the main ore-bearing stratum in the study area. As the parent rocks had high uranium contents, the weathering of these rocks

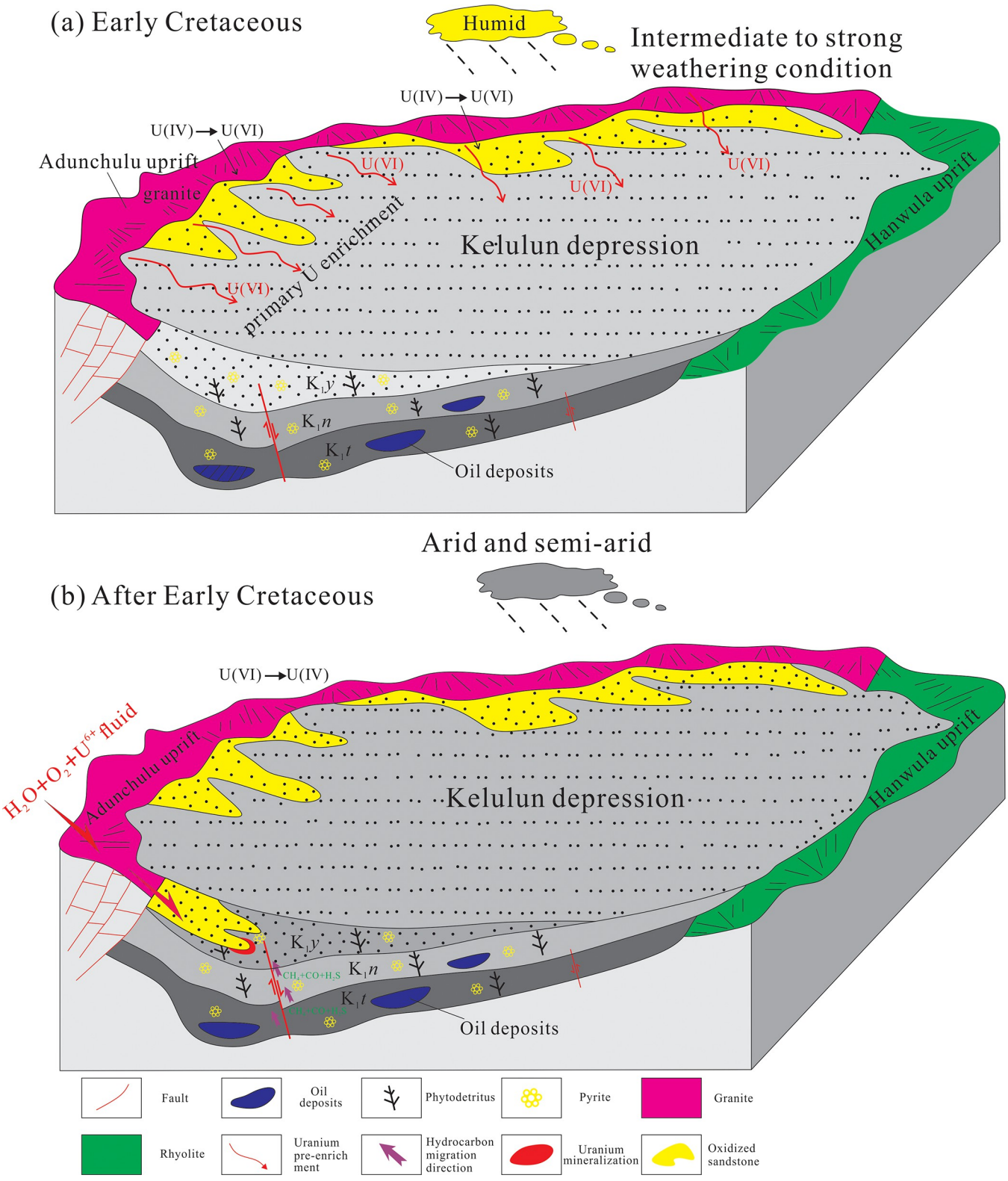

Fig 19. Stages of uranium mineralization in the sandstone uranium deposits of the Kelulun Depression [20].

https://doi.org/10.1371/journal.pone.0309433.g019

created large quantities of uranium-containing clasts, which then migrated into and deposited inside the depression. This effectively "pre-enriched" the strata of the Yimin Formation with relatively high levels of uranium (Fig 19A).

Tectonic inversion at the end of the Early Cretaceous–Late Cretaceous: At the beginning of this period, the extensional setting transformed into a compressional setting, and the sandstone uranium deposits began to form [97]. However, uplifting was less pronounced during this period, which limited the scale of uranium mineralization in the Yimin Formation. At the end of the Late Cretaceous, the Lower Cretaceous strata in the study area underwent compressional deformation, which caused large-scale uplifting and denudation in the Yimin Formation. This increased its hydraulic gradient and thus increased the recharge, runoff, and discharge of supergene fluids [98], which facilitated the infiltration of oxygenated uranium-containing waters into the Yimin Formation. As the Yimin Formation was also rich in reducing matter, such as detrital coal and pyrite, the U(VI) ions in the aforementioned fluid were reduced to U(IV) in its strata, which led to the formation of uranium orebodies in its redox transition zones (Fig 19B).

Basin shrinkage in the Paleogene–Neogene: The tectonic setting in the study area became stable, as the compressional stress became very weak [95,98]. The study area showed a tertiary planation surface, and the Yimin Formation was gradually modified by oxygenated uranium-containing waters, which increased uranium mineralization in its sandstone uranium deposits.

6. Conclusion

1. The Yimin Formation in the Kelulun Depression is mainly comprised of detrital sandstones with low compositional maturity. Based on the geochemical characteristics of these sandstones, the parent rocks are ACM felsic igneous rocks. The parent rocks have undergone a moderately high degree of weathering. The consequent denudation of these rocks provided an ample source of detrital matter in the study area.
2. The detrital zircon U-Pb ages of Yimin Formation sandstones range from 215 Ma to 287 Ma, with a peak at 230–260 Ma. Based on the zircon U-Pb ages, lithology, and geochemical characteristics of these sandstones, it was determined that the Yimin Formation matter was derived from Triassic granites in the Adunchulu Uplift, on the western side of the Kelulun Depression.
3. The Adunchulu Uplift is an outstanding source of uranium. Its uplift since the late Early Cretaceous and subsequent weathering and denudation of its uranium-rich granites played a crucial role in the formation of sandstone uranium deposits. The Kelulun Depression is a promising area for the exploration of sandstone uranium deposits.

Supporting information

S1 Table. Major element data of the Yimin Formation (%). Major element data.
(XLSX)

S2 Table. Trace and rare earth elements data of the Yimin Formation (ppm). Trace and rare earth elements data.
(XLSX)

S3 Table. Detrital zircon U-Pb isotope data of the Yimin Formation sandstones. Detrital zircon U-Pb isotope data.
(XLSX)

S4 Table. Detrital zircon trace element data of the Yimin Formation (ppm). Detrital zircon trace element data.
(XLSX)

Acknowledgments

Firstly, we would like to thank the editors of *PLOS ONE* editorial department for their contributions to this paper. Secondly, we would like to thank all of the participants who took part in the study.Finally, Special thanks go to the anonymous reviewers for their helpful suggestions and comments.

Author Contributions

Data curation: Da Sun.

Formal analysis: Fengjun Nie.

Funding acquisition: Fengjun Nie, Xin Zhang.

Investigation: Fei Xia, Wenbo Zhou, Qing Wang.

Methodology: Wenbo Zhou.

Project administration: Zhaobin Yan.

Resources: Zhaobin Yan.

Software: Xin Zhang.

Writing – original draft: Fanmin Meng.

Writing – review & editing: Fanmin Meng.

References

1. Hall S.M, Mihalasky M.J, Tureck K.R. Genetic and Grade and Tonnage Models for Sandstone-hosted Roll-type Uranium Deposits, Texas Coastal Plain, USA. Ore Geology Review. 2016; 80, 716–753. https://doi.org/10.1016/j.oregeorev.2016.06.013.
2. Cheng Y.H, Wang S.Y, Jin R.S. Global Miocene Tectonics and Regional Sandstone Style Uranium Mineralization. Ore Geology Review. 2019; 106, 238–250. https://doi.org/10.1016/j.oregeorev.2019.02.003.
3. Zhang C, Wang S.B, Yu R.AOccurrence of Uranium Minerals in the Xiaomeigou Formation in Northern Qaidam Basin, Northwest China. Ore Geology Review. 2022; 142, 104692. https://doi.org/10.1016/j.oregeorev.2021.104692.
4. Hu P, Jiao Y.Q, Dong F.S, Guo X.D. Relationships between uranium occurrence, pyrite and carbonaceous debris in the Songliao Basin: Evidenced by mineralogy and sulfur isotopes. Ore Geology Review. 2022; 140, 104580. https://doi.org/10.1016/j.oregeorev.2021.104580.
5. Liu Y, Jun H.Z, Jiao Y.Q, Liu Z.R, Zhou M.F. Constrains of in-situ S-isotopic compositions of pyrite on the genesis of the Bayinqinggeli sandstone-hosted uranium deposit, Ordos Basin, Northern China. Ore Geology Review. 2023; 161, 105608. https://doi.org/10.1016/j.oregeorev.2023.105608.
6. Sun Y.H, Jiao Y.Q, Cuney M., Wu L.Q, Mercadier J, Rong H, et al. Sulfur isotope and trace element constraints on the conditions of pyrite formation from the Diantou-Shuanglong sandstone-hosted uranium deposit, Ordos Basin, China: Implications for uranium mineralization. Ore Geology Review. 2024; 165, 105921. https://doi.org/10.1016/j.oregeorev.2024.105921.
7. Zhang C.Y, Nie F.J, Jiao Y.Q, Deng W, Peng Y.B, Hou S.R, et al. Characterization of Ore-forming Fluids in the Tamusu Sandstone-type Uranium Deposit, Bayingebi Basin, China: Constraints from Trace Elements, Fluid Inclusions and C-O-S Isotopes. Ore Geology Review. 2019; 111, 102999. https://doi.org/10.1016/j.oregeorev.2019.102999.
8. Nie F.J, Yan Z.B, Feng Z.B, Li M.G, Xia F., Zhang C.Y, et al. Genetic models and exploration implication of the paleochannel sandstone-type uranium deposits in the Erlian Basin, North China, A review and

comparative study. Ore Geology Review. 2020; 127, 103821. https://doi.org/10.1016/j.oregeorev.2020.103821.

9. Rong H, Jiao Y.Q, Liu W.H, Cao M.Q, Yu J.X, Wu L.Qet al. Effects of Basic Intrusions on REE Mobility of Sandstones and Their Geological Significance: A Case Study from the Qianjiadian Sandstone-hosted Uranium Deposit in the Songliao Basin. Applied Geochemistry. 2021; 120, 104665. https://doi.org/10.1016/j.apgeochem.2020.104665.
10. Lu M, Ye R, Zhang B.M. Source identification of the geochemical anomaly from the fine-grained soil survey in the Nuheting sandstone-type uranium deposit, Erlian Basin, north China. Journal of Geochemical Exploration. 2021; 227, 106797. https://doi.org/10.1016/j.gexplo.2021.106797.
11. Dimitrios R, Raymond M, Michel C. Olivier P, Marc B. Conditions for uranium biomineralization during the formation of the Zoovch Ovoo roll-front-type uranium deposit in East Gobi Basin, Mongolia. Ore Geology Review. 2021; 138, 104351. https://doi.org/10.1016/j.oregeorev.2021.104351.
12. Fu X.F, Chen Z, Yan B.Q. Analysis of Main Controlling Factors for Hydrocarbon Accumulation in Central Rift Zones of the Hailar-Tamtsag Basin Using a Fault Caprock Dual Control Mode. Science China Earth Sciences. 2013; 56(08), 1357–1370. https://doi.org/10.1007/s11430-013-4622-5.
13. Huang S.H, Qin M.K., Zhou W.B, Liu Z.Y, Liu T, Zhao Z.W, et al. Metallogenic Conditions, Characteristics and Genesis of Sandstone-type Uranium Deposit of the Lower Member of Yimin Formation in Kelulun Sag of Inner Mongolia, China. Journal of Earth Sciences and Environment. 2020; 42(02), 199–214. https://doi.10.19814/j.jese.2019.12013.
14. Ma H.F, Luo Y, Li Z.Y, Qin M.K, Wang. Characteristics of Sandbodies in Zalailuoer depression and analysis of uranium exploration direction. Uranium Geology. 2011; 27(01), 30–35. https://doi.org/1000-0658(2011)01-0030-06.
15. Zhang H.Y, Gao B, Ge Q, Hua E.X. Huang S.H., Yi Let al. The distribution and enrichment of Uranium in groundwater of Hailar Basin. China Environmental Science. 2021; 41(01), 223–231. https://doi.org/10.19674/j.cnki.issn1000-6923.2021.0027.
16. Zhong Y.Q, Xu Q.X, Gu S.F. Application of Airborne Radioactivity Survey Data in Metallogenic Prospect of Sandstone-type Uranium Deposit in Hailar Basin. Geology and Resources. 2010; 19(04), 319–324. https://doi.org/1671-1947(2010)04-0319-07.
17. Zhang Z.J, Yu X.H, Chen Z.K, Guo Q.Y, Luo Y, Zhang C.H. Evolution of depositional system and uriniferous characteristics of Damoguaihe Formation in Kelulun Sag. Uranium Geology. 2005; 21(01), 23–29. https://doi.org/1000-0658(2005)01-0023-06.
18. Ma H.F, Luo Y, Wang M.T, Qi D., Li J.H., Fang X.H. Analysis on metallogenic conditions of ISL-amenable sandstone-type uranium deposits in Kelulun down-faulted basin, Inner Mongolia. Uranium Geology. 2006; 22(02), 83–89. https://doi.org/1000-0658(2006)02-0083-07.
19. Zhou W.B, Zhang R, Liu T, Mu H.Q, Zhao Z.W, Huang X. Metallogenic Geological Features and Prospective Study for Sandstone-type Uranium Deposit in Bel-Ulson Depression. Northwestern Geology. 2020; 53(03), 201–209. https://doi.org/1067-3504(2019)01-0016-06.
20. Meng F.M, Nie F.J, Xia F, Yan Z.B, Sun D, Zhou W.B, et al. Sedimentary Environment, Tectonic Setting, and Uranium Mineralization Implications of the Yimin Formation, Kelulun Depression, Hailar Basin, China. Journal of Marine Science and Engineering. 2024; 12, 763. https://doi.org/org/10.3390/jmse12050763.
21. Guo F, Liu H.X, Fan W.MEarly Jurassic Subduction of the Paleo-Pacific Ocean in NE China: Petrologic and Geochemical Evidence from the Tumen Mafic Intrusive Complex. Lithos. 2015; 224–225, 46–60. https://doi.org/org/10.1016/j.lithos.2015.02.014.
22. Dai H.K, Zheng J.P, Xiong Q. Deep Lithosphere of the North China Craton Archives the Fate of the Paleo-Asian Ocean. Earth-Science Reviews. 2021; 215, 103554. https://doi.org/10.1016/j.earscirev.2021.103544.
23. Liu H.L, Li Z.Q, Li G, Li J.S, Meng Q, Peng Y, et al. Influences of Pre-Existing Structures on Future Growth and Geometry of Faults: A Case Study of Hongqi Sag, Hailar Basin. Earth Science. 2022; 47(07), 2646–2666. https://doi.org/1000-2383(2022)07-2646-21.
24. Zhang K.F, Deng B, Zhang F.Q, A M.N, Chen H.L, Yang S.F, et al. Determination of Early Stage of Early Cretaceous Compressive Event in Hailar Basin, NE China, and Its Tectonic Significance. Earth Science. 2016; 41(07), 1141–1155. https://doi.org/10.3799/dqkx.2016.094
25. Cui J.P, Zhao J, Ren Z.L, Jin W, Xing L, Wang Y.Q. Geochemical Characteristics of Lower Cretaceous Source Rocks and Thermal History in the Huhehu Depression, Hailar Basin. Earth Science. 2020; 45(01), 238–250. https://doi.org/org/10.3799/dqkx.2018.300.
26. Song J, Liu Z.L, Wang C, Gao X, Liu X.X. Multistage Structural Deformations of a Superimposed Basin System and Its Tectonic Response to Regional Geological Evolution: A Case Study from The Late Jurassic-Early Cretaceous Tanan Depression, Hailar-Tamtsag Basin. Marine and Petroleum Geology. 2019; 110, 1–20. https://doi.org/org/10.1016/j.marpetgeo.2019.06.051.

27. Han Z, Mao A, Chen W, Zhu D.F. Fracture Evolution in Oil-rich Rhyolitic Lavas of the Hailar Basin, Northeastern China. Marine and Petroleum Geology. 2021; 124, 104811. https://doi.org/org/10.1016/j.marpetgeo.2020.104811.

28. Zhu M.Y, Shao L.Y, Sun BYao H.P, Spina A, Ma S.M, et al. Sequence Paleogeography and Coal Accumulation Model in the Fluvio-lacustrine Rift Basin: The Lower Cretaceous of the Huhehu Sag of Hailar Basin, Inner Mongolia (NE China). Marine and Petroleum Geology. 2022; 145, 105879. https://doi.org/org/10.1016/j.marpetgeo.2022.105879.

29. Jia R.K, Liu J.L, Han Q.C, Zhao S.M, Shang N.D, Tang P.Q, et al. Mineral Matter Transition in Lignite During Ashing Process: A Case Study of Early Cretaceous Lignite from the Hailar Basin, Inner Mongolia, China. Fuel. 2022; 328, 125252. https://doi.org/org/10.1016/j.fuel.2022.125252.

30. Zhu J.C, Meng R.Q, Feng Y.L, Yuan H.Q, Wu F.C, Wu H.B, et al. Decoding stratigraphic evolution of the Hailar Basin: Implications for the late Mesozoic tectonics of NE China. Geology Journal. 2020; 55 (30), 1750–1762. https://doi.org/org/10.1002/gj.3563.

31. Huang S.H, Zhou W.B, Dong Y, Qin M.K. Characteristics of Host Sandbody and Its Uranium Metallogenic Potential of the Upper Member of Yimin Formation in Bei'er Depression, Hailar Basin. Northwestern Geology. 2021; 54(02), 166–178. https://doi.org/10.19751/j.cnki.61-1149/p.2021.02.014.

32. Liu Y.S, Gao S, Hu Z, Gao C, Zong K, Wang D.Continental and oceanic crust recycling-induced melt-peridotite interactions in the Trans-North China Orogen: U-Pb dating, Hf isotopes and trace elements in zircons from mantle xenoliths. Journal of Petrology. 2010; 51, 537–571. https://doi.org/org/10.1093/petrology/egp082.

33. Andersen T. Correction of common lead in U-Pb analyses that do not report ^{204}Pb. Chemical Geology. 2022; 192, 59–79. https://doi.org/org/10.1016/S009-2541(02)00195-X.

34. Taylor S.R, Mclennan S.M. The Continental Crust: Its Composition and Evolution Geoscience Texts. Blackwell Scientific Publications. 1985, 1–312. OSTI ID: 6582885.

35. Zhao D.J, Wang X.Q. Geochemical characteristics of the Middle Triassic fine-grained clastic sedimentary rocks in Youjiang Basin and its implications for provenance and tectonic setting. Geotectonica et Metallogenia. 2019; 44, 311–324. https://doi.org/10.16539/j.ddgzyckx.2019.06.009.

36. Sun S.S, McDonough W.F. Chemical and isotopic systematics of oceanic basalts: implications for mantle composition and processes. Geol. Soc. Lond, Special Publications. 1989; 42, 313–345. https://doi.org/org/10.1144/GSL.SP.1989.042.01.09.

37. Haskin L.A and Paster T.P. Geochemistry and mineralogy of the rare earths. Handbook on the Physics and Chemistry of Rare Earths. 1979; 3, 1–80. https://doi.org/org/10.1016/S0168-1273(79)03004-X.

38. Kirkland C.L, Smithies R.H, Taylor R.J.M, et al. Zircon Th/U ratios in magmatic environs. Lithos. 2015; 212–215, 397–414. https://doi.org/org/10.1016/j.lithos.2014.11.021.

39. Yu R.A, Li T, Yang T.X, Zhao H.L, Tu J.R, Hu Y.X, et al. Provenance and tectonic evolution of the Middle and Lower Jurassic strata constrains on the uranium mineralization in southwest margin of Ordos Basin. Earth Science. 2023; 1–21. https://doi.org/1000-2383,CN 42-1874/P.

40. Lei W.Y, Shi G.H, Liu Y.X. Research progress on trace element characteristics of zircons of different origins. Earth Science Frontiers. 2013; 20(4), 273–284. https://doi.org/1005-2321(2013)04-0273-12.

41. Belousova E, Griffin W, O'Reilly S Y, et al. Igneous zircon: trace element composition as an indicator of source rock type. Contributions to Mineralogy & Petrology. 2002; 143(5), 602–622. https://doi.org/org/10.1007/s00410-002-0364-7.

42. Zhou Y, Liu Z.L, Kaarel M, Li F.J, Peng N, Kuang H.W, et al. Geochemical characteristics of Jurassic sandstones on the southern margin of the Junggar Basin: Constraints on provenance and sandstone-type uranium mineralization. Ore Geology Review. 2022; 146, 104922. https://doi.org/org/10.1016/j.oregeorev.2022.104922.

43. Sebastian Z, Robert H. Provenance of Cretaceous sandstones in the Banda Arc and their tectonic significance. Gondwana Research. 2019; 67, 1–20. https://doi.org/org/10.1016/j.gr.2018.09.008.

44. Zhao X.C, Liu C.Y, Xiao B, Zhao Y, Chen Y.T. Petrography and Geochemistry of the Upper Triassic Sandstones from the Western Ordos Basin, NW China: Provenance and Tectonic Implications. Acta Geologica Sinica. 2019; 93(6), 1835–1849. https://doi.org/org/10.1111/1755-6724.13863.

45. Sun D, Li H.M, Xia F, Nie F.J, Huang G.W, Zhang Z.B, et al. Provenance and Tectonic Setting of the Lower Cretaceous Huanhe Formation in the Northwestern Ordos Basin and Its Implications for Uranium Mineralization. ACS Omega. 2024; 9, 3324−3341. https://doi.org/10.1021/acsomega.3c06163 PMID: 38284064

46. Girty G.H, Ridge D.L, Knaack C. Provenance and depositional setting of paleozoic chert and Argillite, Sierra Nevada, California. Journal of Sedimentary Research. 1996; 66 (1), 107–118. https://doi.org/org/10.1306/D42682CA-2B26-11D7-8648000102C1865D.

47. Schieber J.A. Combined petrographical geochemical provenance study of the Newland Formation, Mid-Proterozoic of Montana. Geological Magazine. 1992; 129(02), 223–237. https://doi.org/org/10.1017/S0016756800008293.

48. Roser B.P, Korsch R.J. Provenance signatures of sandstone-mudstone suites determined using discriminant function analysis of major-element data. Chemical Geology. 1988; 67(1–2), 119–139. https://doi.org/org/10.1016/0009-2541(88)90010-1.

49. Floyd P, Leveridge B. Tectonic environment of the Devonian Gramscatho basin, south Cornwall: framework mode and geochemical evidence from turbiditic sandstones. Journal of the Geological Society. 1987; 144, 531–540. https://doi.org/org/10.1144/gsjgs.144.4.0531.

50. Floyd P.A, Winchester J.A, Park R.G. Geochemistry and tectonic setting of Lewisian clastic metasediments from the Early Proterozoic Loch Maree Group of Gairloch, NW Scotland. Precambrian Research. 1989; 45, 203–214. https://doi.org/org/10.1016/0301-9268(89)90040-5.

51. Gu X.X, Liu J.M, Zheng M.H. Provenance and tectonic setting of the Proterozoic turbidites in Hunan, south China: geochemical evidence. Journal of Sedimentary Research. 2002; 72, 393–407. https://doi.org/org/10.1306/081601720393.

52. Bracciali L, Marroni M, Pandolfi L. Geochemistry and petrography of Western Tethys Cretaceous sedimentary covers (Corsica and Northern Apennines): from source areas to configuration of margins. Special Paper of the Geological Society of America. 2007; 420, 73–93.

53. McLennan S.M, Hemming S, Mcdaniel D.K. Geochemical Approaches to Sedimentation, Provenance and Tectonics. Geological Society of America Special Papers. 1993; 284, 21–40.

54. Shao L, Stattegger K. Sandstone petrology and geochemistry of the Turpan Basin (NW China): Implications for the tectonic evolution of a continental basin. Journal of sedimentary Research. 2001; 71(1), 37–49. https://doi.org/org/10.1306/041800710037.

55. Cullers R.L, Podkovyrov V.N. Geochemistry of the Mesoproterozoic Lakhanda shales in southeastern Yakutia, Russia: implications for mineralogical and provenance control, and recycling. Precambrian Research. 2000; 104, 77–93. https://doi.org/org/10.1016/S0301-9268(00)00090-5.

56. Fang G.Q. $K_2O/(Na_2O+CaO)$-SiO_2/Al_2O_3: One for pushing Discriminant map of plate tectonic background during fault flysch formation. Geology of northwest China Science. 1993; 14(1), 121–125.

57. Roser B.P, Korsch R.J. Determination of tectonic setting of sandstone-mudstone suites using SiO_2 content and K_2O/Na_2O ratio. The Journal of Geology. 1986; 94(5), 635–650. https://doi.org/org/10.1086/629701.

58. Bhatia M.R, Crook K.A.W. Trace element characteristics of gray-wacks and tectonic discrimination of sedimentary basins. Contributions to Mineralogy and Petrology. 1986; 92, 181–193. https://doi.org/org/10.1007/BF00375292.

59. Bhatia M.R. Plate Tectonics and Geochemical composition of sandstones. The Journal of Geology. 1983; 91(6), 611–627. https://doi.org/org/10.1086/628815.

60. Zhao B. Research on the tectonic evolution feature and origin mechanism in Hailar Basin. Daqing Petroleum Institute. 2010.

61. Johnsson M.J. The system controlling the composition of clastic sediments. Geological Society of America Special Papers. 1993; 284, 1–20.

62. Condie K.C, Noll J.P.D, Conway C.M. Geochemical and detrital mode evidence for two sources of Early Proterozoic sedimentary rocks from the Tonto Basin Supergroup, central Arizona. Sedimentary Geology. 1992, 77(1–2), 51–76. https://doi.org/org/10.1016/0037-0738(93)90007-R.

63. Cox R, Low D.R., Cullers R.LThe influence of sediment recycling and basement composition on evolution of mudrock chemistry in the southwestern United States. Geochimica et Cosmochimica Acta. 1995; 59, 2919–2940. https://doi.org/org/10.1016/0016-7037(95)00185-9.

64. Zhang T.F, Cheng X.Y, Wang S.Y, Miao P.S, Ao C. Middle Jurassic-Early Cretaceous drastic paleoenvironmental changes in the Ordos Basin: Constraints on sandstone-type uranium mineralization. Ore Geology Reviews. 2022; 142, 104652. https://doi.org/org/10.1016/j.oregeorev.2021.104652.

65. Nesbitt H.W, Young G.M. Early Proterozoic climates and plate motions inferred from major element chemistry of lutites. Nature. 1982; 299, 715–717. https://doi.org/org/10.1038/j299715a0.

66. Barshad I. The effect of a variation in precipation on the nature of clay minerals formation in soils from acid and basic igneous rocks. In Proceeding International Clay Conference. Jerusalem. Israel: Israel Program for Scientific Translations. 1966; 22, 167–173. INIST identifier GEODEBRGM6818023760.

67. Vande K.P.C, Leake B.E. Petrogranphy and geochemistry of feldspathic and mafic sediments of the northeastern Pacific margin. Transactions of the Royal Society of Edinburgh Earth Sciences. 1985; 76 (4), 411–449. https://doi.org/org/10.1017/S0263593300010646.

68. Li Y, Nie FJ., Jia L.C, Lu S.J, Yan Z.B. Geochemical Characteristics, Palaeoenvironment and Provenance of Uranium-Bearing Sandstone in the Sifangtai Formation, Northern Songliao Basin, Northeast China. Minerals. 2021; 11, 1019. https://doi.org/org/10.3390/min11091019.

69. Fedo C.M, Nesbitt H.W, Young G.M. Unraveling the effects of potassium metasomatism in sedimentary rocks and paleosols, with implications for paleo-weathering conditions and provenance. Geology. 1995; 23(10), 921–924. https://doi.org/org/10.1130/0091-7613(1995)023<0921:UTEOPM>2.3.CO;2.

70. Nesbitt H.W, Young G.M. Prediction of Some Weathering Trends of Plutonic and Volcanic Rocks Based on Thermodynamic and Kinetic Considerations. Geochimica et Cosmochimica Acta. 1984; 48 (7), 1523–1534. https://doi.org/org/10.1016/0016-7037(84)90408-3.

71. Zhou W.B, Liu T, Mu H.Q, Zhang R Report on results of uranium resource survey and evaluation project in Hailar Basin, Inner Mongolia. Nuclear Industry Group 243rd. 2019.

72. Ma Y.L. Study on sedimentary and reservior characteristics of Bayanhushu Sag. Northeast Petroleum University, 2014.

73. Meng F.M, Nie F.J, Xia F, Du B.H, Yan Z.B, Zhou W. B, et al. Characteristics of chlorite in the Yimin Formation and its relationship with uranium mineralization in the Kelulun Sag, Hailar Basin. Mineralogy and Petrology. 2024, 1–15. https://doi.org/1001-6872,CN 51-1143/TD.

74. Gou J, Sun D.Y, Ren Y.S, et al. Petrogenesis and geodynamic setting of Neoproterozoic and Late Paleozoic magmatism in the Manzhouli-Erguna area of Inner Mongolia, China: Geochronological, geochemical and Hf isotopic evidence. Journal of Asian Earth Sciences. 2013; 67–68, 114–137. https://doi.org/org/10.1016/j.jseaes.2013.02.016.

75. Huang M.D, Zhang H.L, Zhang J.Q, Pei S.L, Huo C, Zhao W.Y.Zircon U-Pb Ages of Three Episodes Mesozoic Granites in the Hailar Basin and Its Significance. J Mineral Petrol. 2018; 38(01), 35–41. https://doi.org/10.19719/j.cnki.1001-6872.2018.01.006.

76. Tian J, Li J.W, Wang R.H, Liu W, An X.P,Kang Y.J,et al. Zircon LA-ICP-MS U-Pb ages and geochemical features of intrusions in Erentaolegai area of Inner Mongolia. Geology in China. 2014; 41(4), 1092–1107. https://doi.org/1000-3657(2014)04-1092-16.

77. Gou J. The Geochronology and Petrogenesis of volcanic rocks in Baiyingaolao Formation from the southern Manzhouli, Inner-Mongolia. Jilin University, 2010.

78. Wang T.H. Geochemistry and Petrogenesis of Late Yanshanian Granites, Southern Manzhouli Area, Inner-Mongolia. Jilin University. 2014.

79. Wang W, Xu W., Wang F, Meng E. Zircon U-Pb Chronology and Assemblages of Mesozoic Granitoids in the Manzhouli-Erguna Area, NE China: Constraints on the Regional Tectonic Evolution. Geological Journal of China Universities. 2012; 18(01), 88–105. https://doi.org/1006-7493(2012)0088-18.

80. Han F, Wang L.L, Zhang Z.GTian M.Z, Wang L. Zircon U-Pb dating of Adunchulu granite in Hulun Buir Geopark of Inner Mongolia, and its tectonic significance. Journal of Arid Land Resources and Environment. 2017; 31(05), 132–135. https://doi.org/10.13448/j.cnki.jalre.2017.156.

81. Wang L. The Geochronology and Petrogenesis of Adunchulu Granites in Xinbaerhu Right Banner, Inner Mongolia. China University of Geosciences (Beijing), 2016.

82. Gou J., Geochronology petrogenesis and tectonic setting of Mesozoic volcanic rocks, southern Manzhouli area, Inner Mongolia. Jilin University, 2013.

83. Sun D.Y, Wu F.Y, Gao S, Lu X.P. Confirmation of two episodes of A-type granite emplacement during Late Triassic and Early Jurassic in the central Jilin Province, and their constraints on the structural pattern of Eastern Jilin-Heilongjiang Area, China. Earth Science Frontiers. 2005; 12(2), 263–275. https://doi.org/1000-0569/2011/027(10)-3083-94.

84. Xu W.L, Wang F, Pei F.PMeng E, Tang J, Xu M.J, et al. Mesozoic tectonic regimes and regional ore-forming background in NE China: Constraints from spatial and temporal variations of Mesozoic volcanic rock associations. Acta Petrologica Sinica. 2013; 29(2), 339–353. https://doi.org/1000-0569/2013/029(02)-0339-53.

85. Zhang S.Y. Geochemical Characteristics and Petrogenesis of the Middle Permian Granites in New Barag Right Banner, Inner Mongolia. Uranium Geology. 2019; 35(06), 343–350. https://doi.org/10.3969/j.issn.1000-0658.2019.06.003.

86. Liu H.J, Jin R.S, Xu Z.L, Tang C, Duan M, i P, et al. Provenance evolution of the Late Cretaceous Uranium-bearing sediments in the southern Daqing placanticline of the northern Songliao Basin Evidence from detrital zircon U-Pb chronology. China Geology. 2022; 33, 1–29. https://doi.org/1000-3657,CN 11-1167/P.

87. Jiao Y.Q, Wu L.Q, Peng Y.B, Rong H, Ji D.M, Miao A.S, et al. Sedimentary tectonic setting of the deposition-type uranium deposits forming in the Paleo-Asian tectonic domain, North China. Earth Science Frontier. 2015; 22, 189–205. https://doi.org/10.13745/j.esf.2015.01.016.

88. Xia Y.L, Liu H.B. Research on supplying potential of Uranium source from rocks. Uranium Geology. 2006; 22(02), 99–103. https://doi.org/1000-0658(2006)02-0099-05.

89. Wang W.Q, Liu C.Y, Wang J.Q, Ma H.H, Guan Y.Z. Characteristics of uranium content and its geological and mineralization significance for the provenance areas, northern northwest China. Earth Science Frontier. 2019; 26, 292–303. https://doi.org/10.13745/j.esf.sf.2018.9.1.

90. Huang G.W, Pan J.Y, Xia F, et al. Provenance of uranium mineralization of the Yuqia area, Northwest China: Constraints from detrital zircon U-Pb geochronology and Hf isotopes. Journal of Earth Science. 2022; 33(6), 1549–157. https://doi.org/org/10.1007/s12583-022-1654-9.

91. Chen J.L. Research of Structural Feature and Structural Evolution in The Hailar-Tamtsag Basin. Chendu University of Technology. 2011.

92. Ji Z, Ge C W. Yang H, Bi J.H, Yu Q, Dong Y. The Late Triassic Andean-type andesite from the central Great Xing'an Range: Products of the southward subduction of the Mongol-Okhotsk oceanic plate. Acta Petrologica Sinica. 2018; 34(10), 2917–2930. https://doi.org/1000-0569/2018/034(10)-2917-30.

93. Chen J.L, Wu H.Y, Zhu D.F, Lin C.H, Yu D.S. Tectonic evolution of the Hailar basin and its potentials of oil gas exploration. Chinese Journal of Geology. 2007; 42(1), 147–159. https://doi.org/0563-5020(2007)01-0147-13.

94. Zhang L.T. The tectonic characteristics and its effect on the control of the oil and gas accumulation in Bayanhushu Sag. Northeast Petroleum University, 2013.

95. Zhao Y. Controlling Factors of oil-gas Accumulation and favorable targets prediction in Bayanhushu Sag. Northeast Petroleum University, 2018.

96. Sun X.M, Lu B.L, Zhang M.S, Du J.Y, Xu Q.W, Tian J.X. Typical Structural Styles and Deformation Sequence in Outcrop Area of Hailar Basin and Its Margin. Journal of Jilin University (Earth Science Edition). 2011; 41(S1), 1–8+23. https://doi.org/1671-5888(2011)Sup.1-001-08.

97. Yang X. Recovery of the prototype basin and structural evolution for Bayanhushu Sag. Petroleum Geology & Oilfield Development in Daqing. 2020; 39(01): 18–25. https://doi.org/10.19597/J.ISSN.1000-3754.201905032.

98. Shang Y, Chen J L, Lin C.H, Fan L.G.Characteristics of late cretaceous tectonic inversion for China Northeast Basin group. Petroleum Geology & Oilfield Development in Daqing. 2021; 40(04), 26–31. https://doi.org/10.19597/J.ISSN.1000-3754.202009017.